Towards the Operational Weather Forecasting Application of Atmospheric Stability Products Derived from NUCAPS CrIS/ATMS Soundings

Flavio Iturbide-Sanchez, *Member, IEEE,* Silvia R. Santos da Silva, Quanhua Liu, Kenneth L. Pryor, Michael E. Pettey, and Nicholas R. Nalli, *Member, IEEE*

***Abstract*—Atmospheric soundings from radiosondes are critical for the weather forecasting, particularly for the diagnostic of atmospheric stability conditions that can lead to thunderstorm development. However, radiosonde observations (RAOBs) are temporally and spatially limited throughout the globe, promoting the use of satellite measurements. This study assesses the applicability to the operational short-term weather forecasting of atmospheric stability indices and parameters (SIPs) derived from thermodynamic profiles retrieved from the National Oceanic and Atmospheric Administration (NOAA) Unique Combined Atmospheric Processing System (NUCAPS) using the Suomi National Polar-orbiting Partnership (SNPP) Cross-track Infrared Sounder (CrIS) and Advanced Technology Microwave Sounder (ATMS) radiances. For this purpose, we validated NUCAPS SIPs against SIPs derived from conventional and dedicated/reference RAOBs collocated with NUCAPS retrievals within a maximum radius of 50 km and ±1-h time difference, over midlatitudes (60ºN to 30ºN) and tropics (30ºN to 30ºS). Stability parameters evaluated include Total Precipitable Water, Lifted Index, K-Index, Total-Totals Index, and Galvez-Davison Index. NUCAPS TPW exhibited the highest level of statistical agreement with RAOBs, with the remaining NUCAPS SIPs exhibiting favorable results (linear correlations ranging between 0.65 and 0.85). Case studies over the Texas/Oklahoma region and the Northern Coast of Brazil demonstrate NUCAPS capability of generating reliable fields of atmospheric stability, as well as capturing synoptic-scale convective signatures, not feasible with RAOBs. Considering also the benefit of SNPP NUCAPS hyperspectral-infrared and microwave soundings available for both regions during critical early afternoon periods, our analysis supports the use of NUCAPS CrIS/ATMS SIPs as complementary nowcasting tools for the analysis of preconvective environments.**

This work was supported by the Joint Polar Satellite System Program Office. (Corresponding author: Flavio Iturbide-Sanchez). The second author was supported by the CAPES Foundation/Ministry of Education of Brazil under grant 88888.075925/2013-00.

F. Iturbide-Sanchez, M. E. Pettey, and N. R. Nalli are with the I. M. Systems Group, NOAA/NESDIS/Center for Satellite Applications and Research, College Park, MD 20740 USA (e-mail: flavio.iturbide@ noaa.gov; michael.pettey@noaa.gov; nick.nalli@noaa.gov).

S. R. Santos da Silva is with the Department of Atmospheric and Oceanic Science/Earth System Science Interdisciplinary Center, University of Maryland, College Park, MD 20740 USA (e-mail: silviare@umd.edu).

Q. Liu, and K. L. Pryor are with the NOAA/NESDIS/Center for Satellite Applications and Research, College Park, MD 20740 USA (e-mail: quanhua.liu@ noaa.gov; ken.pryor@noaa.gov).

Index Terms—**Atmospheric soundings, cross track infrared sounder/advanced technology microwave sounder (CrIS/ATMS), infrared retrievals, microwave retrievals, NUCAPS, remote sensing, satellites, stability indices, weather forecasting.**

I. Introduction

For decades, atmospheric stability indices (SIs) computed from operational radiosonde profiles have been routinely used by weather forecasters to identify convective unstable environments that can potentially lead to thunderstorm development and their consequent hazards, such as heavy rain, strong wind gusts, hail, lightning, and even tornadoes. With the advent of sophisticated sounding instruments aboard environmental satellites and the development of retrieval algorithms using infrared (IR) and microwave (MW) observations, high-quality atmospheric vertical temperature and moisture profiles (AVTPs and AVMPs) have become available, showing potential for thermodynamic analysis applications. In this paper, AVTPs and AVMPs generated by the National Oceanic and Atmospheric Administration (NOAA) Unique Combined Atmospheric Processing System (NUCAPS) were used to derive an ensemble of atmospheric stability indices and parameters (SIPs) of interest for operational weather forecasting. The retrieval algorithm has been applied successfully in a number of polar-orbiting satellite IR/MW sensor suites, including the Atmospheric InfraRed Sounder (AIRS)/Advanced Microwave Sounding Unit (AMSU) suite onboard the National Aeronautics and Space Administration (NASA) Aqua, the Infrared Atmospheric Sounding Interferometer (IASI)/AMSU/Microwave Humidity Sounder (MHS) suite on the European Organisation for the Exploitation of Meteorological Satellites (EUMETSAT) Meteorological Operational (MetOp) -A and -B, and the Cross-track Infrared Sounder (CrIS)/Advanced Technology Microwave Sounder (ATMS) suite of instruments on the Suomi National Polar-orbiting Partnership (SNPP). The present study utilizes operational NUCAPS version 1.5 products generated by the processing of the SNPP CrIS and ATMS radiances. The SNPP spacecraft, launched on October 28th 2011, is part of the Joint Polar Satellite System (JPSS), the United States (U.S.) polar-orbiting operational satellite mission [1]. Its follow-on, JPSS-1 (re-named NOAA-20), was successfully launched on November 18th 2017.

In this work, we explore SIPs derived from SNPP CrIS/ATMS NUCAPS retrievals with the purpose of evaluating their overall applicability as additional tools in the operational weather forecasting routine. The usage of NUCAPS offers the advantage of increasing the spatial coverage of thermodynamic profiles necessary for the atmospheric stability evaluation over data sparse regions or where the density of upper air stations is low (like Africa or Latin America). There is also an impact on the temporal resolution, since operational balloon launch times are commonly limited to 00 and 12 Universal Coordinated Time (UTC). In this case, NUCAPS could provide additional samples of thermodynamic vertical profiles between operational balloon launches, especially during critical afternoon periods when severe convection often initiates over the central U.S. In this region the SNPP overpass times are around 1400 local time (LT) given that the SNPP platform operates in an orbit that crosses the equator at 1330 LT in ascending mode. It should also be noted that the SNPP daytime measurements are taken in the early afternoon times over several regions around the globe. In this sense, the benefit of using NUCAPS in the short-term forecasting of convective activity extends to global scales.

Previous applications of satellite-derived SIPs have been reported in the literature. Some important contributions were inherited from the Geostationary Operational Environmental Satellite (GOES) sounders. Early works used the 12-channel Visible Infrared Spin Scan Radiometer (VISSR) Atmospheric Sounder (VAS) [2]. Some VAS derived parameters like the Total Precipitable Water (TPW), Total-Totals index (TT) and Lifted index (LI), were applied to the analysis of preconvective environments [3]–[5]. From that point, there has been a constant evolution of GOES sounders and retrieval algorithms until the GOES 13-15 series, with 18 IR spectral bands. This has allowed more accurate thermodynamic profiles and has increased nominal spatial (about 10 km) and temporal resolution (currently hourly frequency) of derived stability products [6]–[9]. The recently launched GOES-16 is expected to maintain the capability of deriving legacy stability products from the GOES 13-15 series in spite of not carrying an IR sounder. These products will be generated from the Advanced Baseline Imager (ABI) data through a methodology that requires a numerical model initial profile, but their performance is expected to be slightly degraded relative to the current generation of stability products derived from the GOES 13-15 series [10], [11]. Airmass parameters such as the LI, TPW and K-Index (KI) have also been derived from vertical thermodynamic profiles generated by the Spinning Enhanced Visible and Infrared Imager (SEVIRI), onboard the Meteosat Second Generation (MSG) satellites - the geostationary satellites operated by the EUMETSAT - as described by [12]. The MSG SEVIRI channels used by the physical retrieval algorithm were: three longwave radiation window channels (8.7, 10.8, and 12.0 μm), two water vapor channels (6.2 and 7.3 μm), and the CO_2 channel (13.4 μm).

Despite continuous progress, the usage of multi-channel sounders data from geostationary satellites suffers constraints due to limited spectral resolution and availability of retrieved profiles generally under clear-sky conditions. Efforts towards obtaining retrieved profiles from GOES IR sounder measurements under cloudy conditions have been done (example see [13]). Within this context, JPSS polar-orbiting satellites (beginning with SNPP) offer added capabilities over geostationary satellites due to the inclusion of the ATMS, a passive MW sensor. The operation of the ATMS, collecting surface and atmospheric MW radiances even over cloudy conditions, in conjunction with the high spectral information provided by the IR hyperspectral sounder CrIS (1305 channels at nominal spectral resolution and 2211 channels at full spectral resolution) constitutes one of the key advancements achieved by this generation of satellites. Moreover, the very high spectral resolution of the CrIS measurements results in additional benefits for forecasting applications. These include 1) more accurate profiles with larger vertical resolution allowing better characterization of the thermodynamic structure of the atmosphere, and 2) the first-guess profiles for the physical iterations within NUCAPS do not rely on numerical model forecasts leading to independent soundings useful for model comparison purposes.

An overview of the sounding instruments and the NUCAPS retrieval system is presented in Section II, whereas Section III reviews relevant background on atmospheric stability. Section IV describes the methodology and data sets used herein. Section V presents an analysis of the utility of the NUCAPS-derived SIPs, including statistical assessments versus collocated radiosonde observations (RAOBs), followed in Section VI by an analysis of the performance of NUCAPS-based SIPs over selected cases where convective weather conditions ensued. Section VII provides the main conclusions of this work.

II. Background

A. Advanced Technology Microwave Sounder (ATMS)

The ATMS is a cross-track scanning radiometer with 22 channels covering four MW spectral bands: K (23.8 GHz)/Ka (31.4 GHz), V (50.3–57.3 GHz), W (88.2 GHz), and G (165–183 GHz) [1]. The ATMS was devised to have most of the sounding channels from its predecessors AMSU Unit-A1 (AMSU-A1), Unit-A2 (AMSU-A2), Unit-B (AMSU-B), and MHS, operating on the POES-series satellites since the NOAA-15 (launched in 1998), the MetOp-A/MetOp-B satellites (launched in 2006 and 2012, respectively), and the Aqua platform (launched in 2002). However, the ATMS instrument includes one additional temperature channel at 51.76 GHz, and two new water vapor sounding channels (19 and 21) to ameliorate the thermodynamic characterization of the low to middle troposphere [14]. As a result of the ATMS channel selection, channels 1-16 are primarily designed to profile the atmospheric temperature from the surface to about 1 hPa (~45 km), whereas channels 17-22 are designed for humidity soundings from the surface to about 200 hPa (~15 km) [15].

Another crucial advance lies on the larger ATMS scan angle of ± 52.725º (versus ± 48.3º for AMSU-A) from the nadir direction. For all ATMS channels, measurements are taken every 1.11º (angular sampling interval) at 96 Earth-viewing angles per scan line. This results in a wider swath width of ~2500 km. In consequence, ATMS can operate without orbital gaps poleward of 20º, and shows increased coverage within

the 20°S-20°N region in comparison to its predecessors [14]. It should also be noted the better horizontal resolution of ATMS channels 3-16 of about 32 km at nadir (versus about 47 km for the equivalent AMSU channels 3-15), as well as the high vertical resolution (3 to 6 km, approximately) of the temperature and moisture profiles derived from measurements of the ATMS channels 3-15 and 17-22, respectively [1], [14]. For ATMS channels 17-22, which have a beam size of 1.1 degrees, the horizontal resolution ameliorates to nearly 16 km at nadir. Finally, the static beam width of 5.2 degrees for ATMS channels 1-2 leads to a footprint size close to 75 km at nadir. However, for purposes of processing by the NUCAPS, ATMS observations must be re-sampled to match the CrIS configuration scan geometry during the NUCAPS pre-processing step [16], [17]. In this step, the ATMS scan sets are basically synchronized with those of the CrIS instrument.

B. Cross-track Infrared Sounder (CrIS)

The Cross-track Infrared Sounder (CrIS) is a Fourier transform spectrometer with 1305 sounding channels, when operating at nominal spectral resolution, distributed among three IR spectral bands corresponding to longwave (LWIR: 650-1095 cm^{-1}), midwave (MWIR: 1210-1750 cm^{-1}), and shortwave (SWIR: 2155-2550 cm^{-1}) [1].

CrIS is part of the recent generation of hyperspectral IR sounders that have caused an unprecedented revolution in atmospheric sounding capability. Such generation of advanced sounders also includes the AIRS on the Aqua platform and the IASI onboard the MetOp-A/MetOp-B satellites. In common, these instruments possess enhanced sounding capability due to their high spectral resolution and large number of spectral channels. As shown in [18], the large number (typically thousands of measurements) of noise independent spectral channels of radiance provides an order of magnitude improvement in signal to noise ratio in comparison with multi-spectral sounders (holding 2 to 50 spectral channels).

In particular, CrIS allows the derivation of vertical profiles of temperature and moisture with vertical resolution ranging between 1 to 2 km in the troposphere, and 3 to 5 km in the stratosphere [1]. Recent studies have reported levels of radiometric uncertainty better than the requirements for the JPSS program [19]. Furthermore, CrIS offers the advantage of the lowest noise level in comparison to IASI and AIRS [20], [21].

CrIS scanning geometry is based on a 2200 km swath width (full Earth view scan angle of +/-48.3°). Each scan sweep occurs in the cross-track direction, in which CrIS measures a total of 30 fields of regard (FORs) along each scan line every 8s. For each of the three IR bands, one FOR consists of nine fields-of-view (FOVs), forming a 3 × 3 array of circles whose centers are separated by 1.1° (approximately 16 km at nadir). Since one FOV corresponds to a nadir spatial resolution of about 14 km, a FOR corresponds to a footprint size of around 50 km at nadir [22].

C. The NOAA Unique Combined Atmospheric Processing System (NUCAPS)

NUCAPS is the official NOAA system retrieving vertical temperature, and water vapor profile environmental data records (EDRs) from the processing of CrIS and ATMS sensor data records (SDRs). The suite of NUCAPS EDR products includes retrieved estimates of vertical profiles of atmospheric temperature (AVTP), water vapor (AVMP), and trace gases, under non-precipitating conditions.

The inversion algorithm is based upon the NASA AIRS Science Team Retrieval algorithm documented in [23], [24], and was first implemented at NOAA in 2002 to process AIRS/AMSU data. Further development led to a code with a modular architecture capable of processing data from multiple sensors. This is done by the pre-processing of the SDRs into a common binary file format, which means that the input file to the retrieval code is rigorously the same. Hence, the same retrieval algorithm has been currently used at the NOAA National Environmental Satellite, Data, and Information Service (NESDIS) Center for Satellite Applications and Research to process the Aqua/AIRS/AMSU suite, the MetOp-A/IASI/AMSU/MHS suite (operational since 2008), and more recently the SNPP/CrIS/ATMS suite (operational since 2014).

NUCAPS processing structure comprises of six main modules, which are described in detail by [16], [25]. The NUCAPS IR/MW physical retrieval module uses a multi-step and iterative scheme, where the state variables are solved sequentially at each step using cloud-cleared radiances. While solving for the geophysical variable to be determined at each step, the retrieval system keeps fixed the other variables. The solution (least square minimization) to each step, and iteration, *i*, is done in the form of (1) for temperature, and (2) for water vapor [16], [23],

$$\mathbf{T}_{i+1} = \mathbf{T}_i + \mathbf{F}\Delta\mathbf{A}_{i+1} \tag{1}$$

$$\mathbf{q}_{i+1} = \mathbf{q}_i\left(1 + \mathbf{F}\Delta\mathbf{A}_{i+1}\right) \tag{2}$$

where, $\mathbf{F}$ represents a set of trapezoids piecewise perturbation functions with dimensionless maximum value of 1.0. NUCAPS solves for the geophysical perturbation parameter $\Delta\mathbf{A}_{i+1}$ in a reduced space, using the eigenvector, $\mathbf{U}_i$, and eigenvalues $\boldsymbol{\lambda}_i$ as given in (3),

$$\Delta\mathbf{A}_{i+1} = \mathbf{U}_i\left(\boldsymbol{\lambda}_i + \Delta\boldsymbol{\lambda}_i\right)^{-1}\mathbf{U}_i^{\,T}\mathbf{K}_i^{\,T}\mathbf{S}_e^{-1}\left[\Delta\boldsymbol{\theta}_i - \boldsymbol{\delta\theta}_i\right] \tag{3}$$

where $\boldsymbol{\lambda}_i = \mathbf{U}_i^{\,T}\left(\mathbf{K}_i^{\,T}\mathbf{S}_e^{-1}\mathbf{K}_i\right)\mathbf{U}_i$, and $\Delta\boldsymbol{\lambda}_i$ is the retrieval damping parameter that limits the propagation of noise into the solution by damping the eigenvalues $\boldsymbol{\lambda}_i$. The $\mathbf{K}_i$ is the sensitivity matrix containing information of the partial derivative of the radiances computed at the *i-th* iteration for each channel with respect to each geophysical parameter as part of the inversion. The damping parameter varies with the atmospheric state, since it depends on the eigenvalues $\boldsymbol{\lambda}_i$, which are updated at each retrieval iteration with the update of the sensitivity matrix K_i [23]. In (3), $\mathbf{S}_e$ denotes the error covariance matrix holding the information of both observational and forward model errors, the parameter $\Delta\boldsymbol{\theta}_i$ is the difference between the cloud-clear column radiances and the radiances computed at the *i-th* iteration, weighted inversely with respect to expected noise levels [23], and $\boldsymbol{\delta\theta}_i$ represents

the fraction of the residual due to the propagation of the first guess, and is therefore defined sometimes as the background radiance term. The NUCAPS IR/MW temperature and water vapor first-guess profiles are derived using a statistical eigenvector regression scheme trained against analyses from the European Center for Medium range Weather Forecasting (ECMWF) model and CrIS cloud-cleared radiances [23], [26].

The NUCAPS IR/MW physical retrieval module uses an optimally selected subset of IR channels [27] in the interest of computational efficiency of the retrieval implementation in an operational environment. In this case, the CrIS spectrum at nominal spectral resolution, consisting of 1305 channels, is replaced by a subset of less than 500 channels. As demonstrated in [27], this channel selection constitutes an optimal channel subset capable of accounting for more than 99% of the total variance across the whole spectrum, except for the 600–700-cm^{-1} and 1700-cm^{-1} regions, where the explained variance is around 95%, and for the 2200–2300-cm^{-1} region, where the explained variance ranges between 85% and 99%.

One key component of the NUCAPS is the cloud clearing module developed to produce cloud-cleared IR radiances by combining a set of ATMS and CrIS channels [16]. This allows the derivation of vertical profiles of temperature and water vapor under non-precipitating conditions (clear, partly cloudy, and cloudy). Recent results have shown the ability of NUCAPS to derive sounding products over nearly 85% of the globe [28]. The use of hyperspectral-IR and MW observations, available on polar-orbiting low-earth-orbiting (LEO) satellites, constitutes a major advancement in relation to the current generation of profiles retrieved from measurements taken by geostationary sounding systems, where hyperspectral-IR and MW observations are not available and soundings are limited to clear sky conditions. The lack of MW sounders in geostationary systems is mostly associated with the requirement of very large antenna aperture needed to provide high spatial resolution soundings of the Earth's atmosphere [29].

In the current study, all IR/MW AVTPs and AVMPs profiles were taken from the operational NUCAPS SNPP CrIS/ATMS EDRs version 1.5, which has a global IR/MW convergence of about 65%. Since each NUCAPS FOR is based upon 9 CrIS FOVs (one CrIS FOR), the horizontal resolution of the NUCAPS AVTPs and AVMPs varies along the CrIS scan line between 50 km at nadir to approximately 70×135 km at the scan edges. It is important to mention that for cases with cloud fraction above 85% and precipitating conditions within the FOR, the IR/MW retrieval typically fails converging to a solution.

III. Atmospheric Stability and Stability Indices

The presence of atmospheric instability conditions and the availability of moisture in the low- or mid-troposphere are two essential components to convective weather development. The existence of a triggering mechanism to provide the lifting of air parcels, until achieving the level of free convection (LFC) (above the LFC, parcels accelerate upward due to a positive buoyancy force), is a third contributor, particularly for deep convection development associated with severe weather [30], [31]. The study of atmospheric stability is anchored on the general concepts of static stability and the parcel method (based on the parcel-to-environment temperature difference assuming a hypothetical air parcel in adiabatic ascent), evolving to related concepts of conditional, absolute, latent and potential/convective instability. These concepts are reviewed in [30]. In this context, most SIs were developed to provide an indication of the first two convective-generating components (individually or coupled) and constitute widely used tools among operational forecasters for very-short-range prediction (a few hours). However, users should be aware of the intended geographical region of application and purpose of each SI. Moreover, local objective performance evaluations providing proper thresholds and their seasonal variations must be performed for applications at different locations [12], [32].

The SIPs selected for this work include the Showalter Index (SWI) [33], LI [34], KI [35], TT [36] and TPW, traditional parameters used by forecasters, as well as the Galvez-Davison Index (GDI) [37], a recently developed index optimized for applications over the tropical and subtropical regions. All previously mentioned SIPs are briefly outlined below. In all cases, T and T_d correspond to the ambient air and dewpoint temperatures, respectively, and their numeric subscripts refer to the pressure levels they must be obtained from.

—Total Precipitable Water (TPW):

TPW (normally given in mm) expresses the depth of liquid water accumulated at the surface if all the water vapor in a column of unit cross section extending from the surface to the top of the atmosphere were condensed and precipitated as rain. The TPW is not a SI per se, however this parameter is largely used in the operational forecasting in combination with other SIs. For example, the LI, which is a measure of the buoyant potential of low-level air parcels, in combination with TPW provides useful information on two essential components for convective development: the existence of conditions that favor atmospheric motions in the vertical direction, and the amount of water vapor in the atmospheric column.

—Showalter Index (SWI):

The SWI was originally developed for applications in the southwestern U.S. related to the occurrence of non-severe convective showers and thunderstorms [30]. It is defined as

$$SWI = T_{500} - T_{P,500} \tag{4}$$

where $T_{p,500}$ is the temperature of an air parcel lifted dry-adiabatically from 850 hPa to its lifting condensation level (LCL) and then moist-adiabatically to 500 hPa. Negative values indicate increased potential for convective activity, especially with $SWI \leq -3^{o}C$.

— Lifted Index (LI):

Defined in (5), the LI was originally utilized in the forecasting of severe thunderstorms and tornadoes in the U.S. [30].

$$LI = T_{500} - T_{P,500*} \tag{5}$$

where $T_{P,500*}$ is computed similarly to $T_{P,500}$, but the parcel is defined as having mean temperature (from the original

sounding or a modified sounding using the predicted maximum temperature) and mean mixing ratio from the lowest 3000-foot layer. Since the lifting parcel has been defined in several ways (see discussion in [38]), we considered the parcel as assuming mean thermal and moisture characteristics of the lowest 100 hPa, which means that the LI depends critically on the sounding information within the planetary boundary layer (PBL). This distinctly differs from the SWI definition in which the lowest level sounding information required is at the 850-hPa level. Thus, the NUCAPS SWI is less dependent on the performance of the NUCAPS retrievals near the surface than the NUCAPS LI. Negative values of the LI are associated with unstable conditions. In this case, the more negative, the more unstable the atmosphere is. For example, $LI \leq -6^{o}C$ indicates very unstable conditions, and very strong potential for thunderstorm development.

—K-Index (KI):

The KI was developed for applications in the U.S. related to the occurrence of non-severe convective showers and thunderstorms [39].

$$KI = \left(T_{850} - T_{500}\right) + T_{d,850} - \left(T_{700} - T_{d,700}\right) \quad (6)$$

The likelihood of showers and thunderstorms increases for higher values of KI. KI > +30ºC is the general threshold of interest for forecasters since it denotes a high probability of occurrence of thunderstorms.

— Total Totals Index (TT):

The TT was conceived to identify areas potentially favorable for severe weather occurrence in the U.S. [30], and is described in (7).

$$TT = T_{d,850} - T_{500} + T_{850} - T_{500} \quad (7)$$

The likelihood of severe development increases for higher values of TT. TT ≥ +44ºC is the suggested threshold over U.S. [39]. As noted in (6) and (7), a common characteristic of TT and KI is that both indices require sounding information at 850 and 500 hPa (KI also requires the 700-hPa level). Hence, the NUCAPS TT and NUCAPS KI, by definition, do not require input data representative of the boundary-layer conditions making them less sensitive to the quality of the NUCAPS retrievals near the surface as compared to the NUCAPS LI, for example.

—Galvez-Davison Index (GDI):

The GDI (unitless) was designed for applications in the tropics and subtropics (including southeastern U.S.), by quantifying three relevant factors that generate and modulate moist tropical convection [37], [40]. Given that traditional indices, like LI and TT, were conceived for application over midlatitudes, in our work, the GDI was particularly selected to assess the forecasting potential of NUCAPS-derived indices over tropical regions. It is defined as:

$$GDI = ECI + MWI + II\left(+ OC\right) \quad (8)$$

where:

- *ECI* corresponds to the equivalent potential temperature proxy (EPTP) core index intended to evaluate the convective instability of the mid-troposphere through the equivalent potential temperature (EPT) vertical profile.
- *MWI* corresponds to the mid-level warming index, which takes into consideration the effects of mid-levels troughs (cold air enhancing instability) and ridges (warm air enhancing stability).
- *II* is the inversion index designed to consider the existence of temperature inversions and dry air entrainment.
- *OC* is an optional correction recommended over elevated mountain ranges when visualization packages using gridded data (e.g., GrADS) are used for plotting.

The computation of GDI requires temperature and mixing ratio data at 950, 850, 700 and 500 hPa (and surface pressure for the OC). The 950-hPa level was particularly selected to include information in the PBL [37]. Hence, the performance of the NUCAPS retrievals within the PBL will play an important role in the quality of the NUCAPS GDI. Increasing GDI values indicate higher potential for thunderstorm development (refer to [37] for the complete interpretation of GDI values).

IV. Data and Methodology

The evaluation methodology is predicated on comparisons between RAOBs with the closest NUCAPS retrievals collocated within a maximum radius of 50 km and ±1-h time difference. Only NUCAPS AVTPs and AVMPs that passed the IR/MW retrieval quality control criteria were used in this study. The collocated RAOBs and NUCAPS profiles were obtained from the NOAA Products Validation System (NPROVS) [41]. RAOBs used in this work derive from two categories: (1) conventional radiosondes launched by the World Meteorological Organization (WMO) upper air stations to support operational weather forecasting; and (2) satellite synchronized dedicated and reference radiosondes, characterized by their optimum accuracy and well-known error characteristic [42].

The evaluation was conducted separately over two latitudinal bands: midlatitudes (60ºN to 30ºN) and tropics (30ºN to 30ºS). Over midlatitudes, collocations with conventional RAOBs from 1 April to 30 September 2015 were used to focus on the warm season. In the case of dedicated/reference RAOBs, collocations were taken from the warm seasons of the years between 2013 and 2016. For the evaluation over the tropics, only conventional RAOBs were used due to the limited number of dedicated/reference RAOBs in this region. In this case, the evaluation based on conventional RAOBs employed all collocation matchups found over the tropics during the December 2014 to December 2015 period. This approach ensured a robust sample of collocations, producing approximately 11100 collocations with conventional RAOBs and 600 matchups against dedicated/reference RAOBs over midlatitudes, and about 4500 collocations against conventional RAOBs over the tropics. Fig. 1 shows the distribution of the conventional and reference/dedicated radiosondes used in this study. Over mid-latitudes (Fig. 1(a)), approximately 62 collocations per day with conventional RAOBs were found within a period of six

months. About 85% of these NUCAPS-RAOB collocations were located in the Eastern Hemisphere (east of the Greenwich meridian), particularly over the Europe. For the collocations over the tropic regions (Fig. 1(b)), about 12 collocations per day were found within a year period. In this case, 70% of the matchups were localized in the Eastern Hemisphere. Regarding the dedicated/reference radiosondes (Fig. 1(c)), about 60% of the matchups were also found in the Eastern Hemisphere. All dedicated/reference RAOBs were performed using the Vaisala RS92 radiosondes. For the conventional RAOBs, Tables I and II report the types of radiosondes used. Further details about the characteristics of the operational radiosondes used in this work can be found in [43].

TABLE I
SUMMARY OF THE CONVENTIONAL RADIOSONDE TYPES[a] USED IN THIS WORK: MIDLATITUDES

Type/Manufacturer (Country)	BUFR Code (Subtype)[b]	Number of Reports
RS80/Vaisala (Finland)	037,060,062	152
RS92/Vaisala (Finland)	079,080,081,114,152	2828
RS41/Vaisala (Finland)	123,141	403
DFM-06,DFM-09/Graw (Germany)	018,117	1546
MRZ,RF95,BAR,RZM,AK2/AVK, Vektor, MARL (Russia)	027,053,058,068,069, 088,089,128,129	2855
LMS-6/L. M. Sippican (U.S.)	111, 182	953
M10/Modem (France)	177	542
12M,22M/PAZA (Ukraine)	115,116	461
VIZ MARK I Microsonde/Jinyang (Korea)	021	235
Others	007,009,026,035,071, 090,096,122,130	1175

[a]The majority of radiosondes in "Others" (1061 reports) refers to the BUFR code 090 used for a mixture of Russian unspecified types mostly made by Aeropribor [43].
[b]The BUFR code is designed to identify each major radiosonde type (and subcategories) in WMO FM 94 BUFR reports. BUFR stands for Binary Universal Form for the Representation of meteorological data.

TABLE II
SUMMARY OF THE CONVENTIONAL RADIOSONDE TYPES[a] USED IN THIS WORK: TROPICS

Type/Manufacturer (Country)	BUFR Code (Subtype)	Number of Reports
RS80/Vaisala (Finland)	037,060,063	320
RS92/Vaisala (Finland)	079,080,081, 114,152	674
RS41/Vaisala (Finland)	123,147	760
DFM-09/Graw (Germany)	117	114
LMS-6/L. M. Sippican (U.S.)	182	513
M2K2-DC,M10/Modem (France)	177	1473
BAT-4G/InterMet (South Africa)	099	268
GTS-1/Shanghai C. M. (China)	131,132,133	134
Others	007,009,055, 090,096,122	245

[a]The majority of radiosondes in "Others" (199 reports) refers to the BUFR code 009 used for unspecified types from unknown manufacturers.

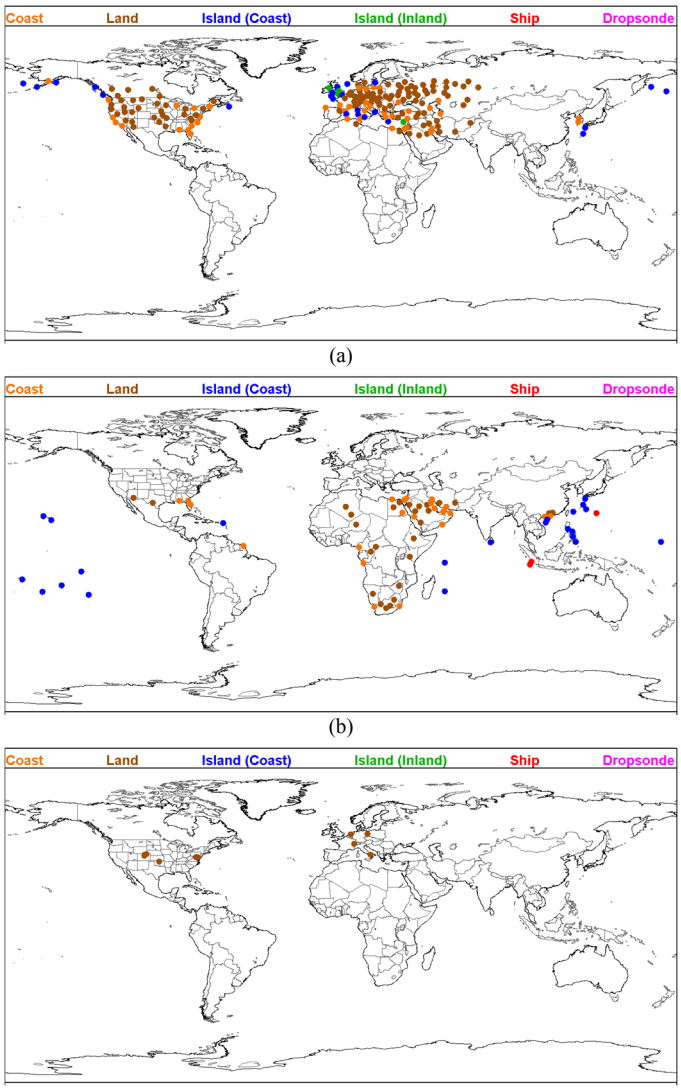

Fig. 1. Spatial distribution of the radiosonde sites where collocations of RAOBs and NUCAPS soundings (within ±1h and 50km) were performed. Different colors denote different terrain types as indicated on the map legend. Collocations with (a) conventional RAOBs over midlatitudes, (b) conventional RAOBs over the tropics and (c) reference/dedicated RAOBs over midlatitudes.

Before proceeding, it is necessary to point out the key aspects regarding the validation of satellite products relative to RAOBs. The statistical results presented in this work include errors stemmed from temporal and spatial collocations as well as intrinsic errors found in the radiosondes instrumentation. Another aspect to consider is the fact that satellites, in reality, provide volume-averaged rather than level-specific observations like the radiosondes, resulting in differences associated with representativeness of the observed atmosphere. Thus, intrinsic differences inevitably exist when comparing SIPs derived from satellite observations against SIPs produced from RAOBs. For example, over regions where large atmospheric inhomogeneities are observed within the satellite field-of-view, SIPs corresponding to an average of the observed atmosphere will be produced by NUCAPS. In contrast, radiosondes provide SIPs only representative of the launch location. However, even this is not strictly speaking true due to representativeness errors associated with the spatial

drift experienced during the radiosonde ascent, which can reach tens to hundreds of kilometers. Since satellites perform nearly instantaneous observations, they do not show this type of representativeness error. These uncertainties contribute to increment the differences found during NUCAPS/RAOBs comparisons. In this respect, we can anticipate that the use of dedicated/reference RAOBs as correlative measurements (Section V-C) improves the overall statistical performance of the NUCAPS SIPs due to their reduced temporal and spatial mismatch/noncoincidence errors as well as their higher-quality sensors.

Given that the NUCAPS IR/MW AVTPs and AVMPs are produced for fixed 100 pressure levels, the removal of those levels below the surface level was made by comparisons with the NUCAPS surface pressure, which is ancillary information acquired from the Global Forecast System (GFS) model and required during the NUCAPS pre-processing. Most SIPs require temperature/moisture content information at specific pressure levels, such as 500, 700, 850, and 950 hPa. Since atmospheric parameters at these specific levels are not provided by the NUCAPS AVTPs/AVMPs products, a linear interpolation scheme was applied. Considering that NUCAPS AVMPs are vertical profiles of mixing ratio, the conversion to dewpoint temperature follows the procedures described in [44]. The code devised for the computation of the LI is based on the work presented in [45].

V. Analysis of NUCAPS-derived stability indices

A. Profile EDR performance – Tropics and Midlatitudes

The global validation and assessment of the NUCAPS temperature and moisture profile EDRs relative to radiosonde data has been detailed in [46], [47], but here we examine the performance of the NUCAPS retrievals relative to standard RAOBs over the regions of interest, namely midlatitudes and tropical zones.

This preliminary evaluation is important since the temperature and moisture profiles constitute the input data for computation of the air stability parameters. For this reason, the analyses are mainly focused on levels of particular interest for such computation. Note that the statistical performances presented in the following analysis include: (1) time and space collocation errors, (2) representativeness errors, and (3) radiosonde instrumentation and sensor errors (reported uncertainties of conventional RAOBs are around 0.5 K for temperature and 10% for relative humidity [48]). Since these errors can be systematic or random, their impact can be reflected in both the bias and standard deviation.

The computation of validation statistics of retrieved thermodynamic profiles relative to RAOBs follows the methodology presented in [42], which establishes the fundamental metrics for the assessment of temperature and water vapor. The initial procedure of the method requires the reduction of the high-resolution RAOB profile to a lower vertical resolution. In this work, the computation of validation statistics are performed on the 100 Rapid Transmittance Algorithm (RTA) layers of the NUCAPS products. Vertical thermodynamic gradients in the lower troposphere contain substantial information for the evaluation of the atmospheric stability. In this sense, it is important to note that the pressure grid resolution of the NUCAPS EDR products in the mid- to the lower troposphere is about 25 hPa. This resolution size is appropriate to resolve steep thermodynamic vertical gradients occurring in the lower atmosphere.

Fig. 2 shows the standard deviation (STD) and the bias statistics (BIAS) calculated from the temperature differences between NUCAPS profiles and conventional RAOBs over midlatitudes and tropics. At midlatitudes, the skill of NUCAPS noticeably decreases downward, particularly near the surface, where BIAS and STD values are around -1.7 K and 3.1 K, respectively. The maximum negative BIAS near the surface indicates an underestimation of NUCAPS retrieved temperatures at those levels (cold BIAS). On the other hand, the BIAS becomes slightly positive between 750 and 400 hPa, where maximum values of about 0.6 K are observed, whereas the STD decreases over these particular pressure levels. The negative BIAS observed between 250 and 350 hPa results from the low ability of NUCAPS to resolve the temperature structure over the tropopause. In comparison to midlatitudes, results over the tropical region show better skill of NUCAPS in retrieving temperature over several pressure levels, particularly near surface. However, the observed tendency of NUCAPS to degrade as approaching the surface is also found. This performance is associated with the complexity in distinguishing atmospheric from surface contributions, when retrieving the atmospheric temperature closer to the surface; and to the limited number of independent pieces of information contained in the satellite observations [27] to sense the high temperature variability found over the PBL in comparison to the high vertical resolution observations performed by the radiosondes. At lower levels (around 850 hPa), NUCAPS exhibits a slight warm BIAS close to 0.5 K over the tropics. Like the midlatitudes case, NUCAPS STD decreases toward the mid-level pressures, having a minimum value near 350 hPa. In summary, NUCAPS shows better bias performance over the tropics, while its capability to retrieve temperature is degraded near the surface, situation that is more pronounced over midlatitudes.

Fig. 3 depicts the STD and BIAS of AVMPs derived from NUCAPS. Unlike the AVTP case, the overall accuracy of the AVMP profiles does not exhibit a degradation as approaching the surface, since it is reported as a relative value given in percent differences (see [42] for in-depth details on this computation). This procedure aims at avoiding the skewing of validation statistics in dry atmospheres (e.g., middle to upper troposphere or polar regions), which would occur when computing the validation metrics using absolute values. The NUCAPS water vapor shows BIAS values around 10% and 5% at 950-hPa over midlatitudes and tropics, respectively. A negative (dry) BIAS is evident in NUCAPS over both regions. In this case, the largest magnitudes of the BIAS computed for the NUCAPS AVMPs are found in the tropics, with values about 14 and 18% for 800 and 500 hPa, respectively.

In Fig. 4 we analyze the statistical performance of the NUCAPS-derived mean parcel (MP) temperature and dewpoint at the lowest 100 hPa, which helps assessing the quality of the NUCAPS soundings in the lower atmosphere. Moreover, both quantities represent indispensable input parameters for the computation of the NUCAPS LI, as defined in Section III. Fig. 4(a) reveals high level of agreement of

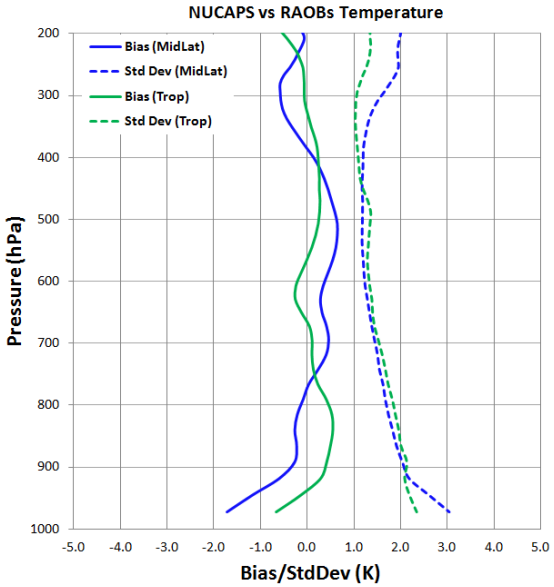

Fig.2. NUCAPS atmospheric vertical temperature profile of BIAS (solid line) and STD (dashed line) statistics relative to conventional RAOBs matchups: (blue) midlatitudes (30ºN to 60ºN) from 1 April to 30 September 2015, and (green) tropics (30ºS to 30ºN) from December 2014 to December 2015.

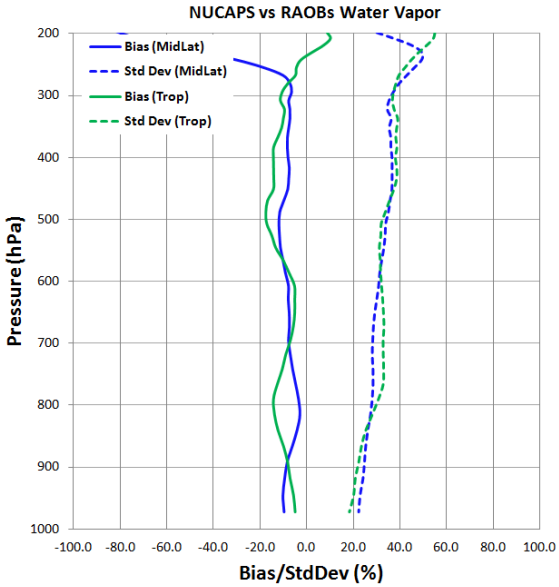

Fig. 3. NUCAPS atmospheric vertical moisture profile of BIAS (solid line) and STD (dashed line) statistics relative to conventional RAOBs matchups: (blue) midlatitudes (30ºN to 60ºN) from 1 April to 30 September 2015, and (green) tropics (30ºS to 30ºN) from December 2014 to December 2015.

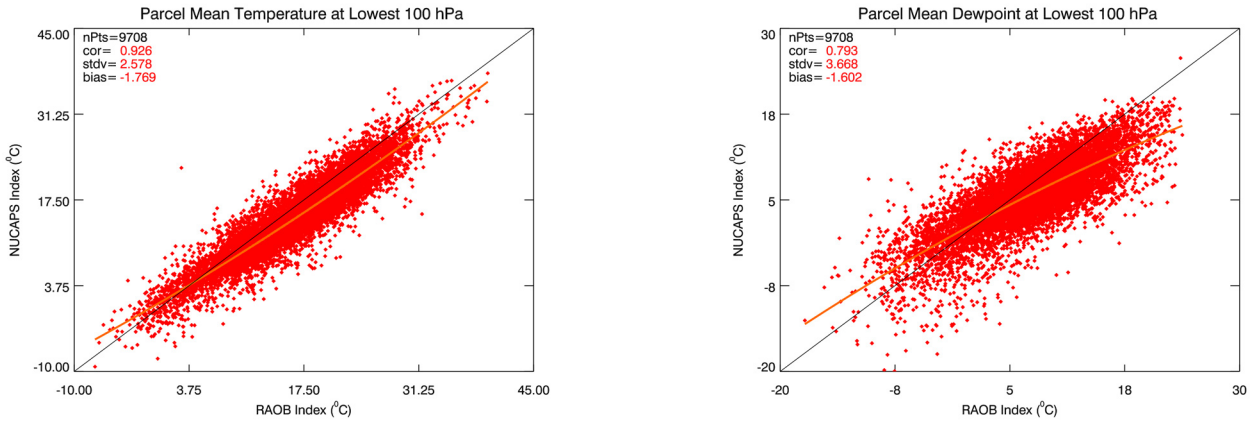

(a) (b)

Fig. 4. Scatterplots of conventional RAOBs versus NUCAPS versions of the Mean Parcel Temperature at Lowest 100 hPa (a) and the Mean Parcel Dewpoint at Lowest 100 hPa (b) for midlatitudes.

NUCAPS MP temperature in relation to RAOBs (linear correlation *r* about 0.93). It can also be observed a negative BIAS of about −1.77ºC in the NUCAPS estimation. This result is in line with the negative BIAS already observed in Fig. 2. For the NUCAPS MP dewpoint (obtained by averaging NUCAPS mixing ratio data from all available levels within 100 hPa of the surface), Fig. 4(b) shows high level of agreement against RAOBs counterparts as indicated by the favorable correlation value of about 0.8. The negative BIAS (about −1.60ºC) results from the negative biases found in the NUCAPS water vapor near the surface, as displayed in Fig. 3. It can also be noted that the NUCAPS STD for dewpoint (near 3.67ºC) is larger than for temperature (about 2.58ºC). Overall, Fig. 4 shows that the NUCAPS-derived MPs tend to be colder and drier than the RAOBs-derived versions. Furthermore, it is observed that the NUCAPS MP temperature is in better agreement with respect to RAOBs than the NUCAPS MP dewpoint.

The assessment of the NUCAPS soundings with respect to conventional RAOBs at pressure levels corresponding to 500, 700, 850, and 950 hPa is presented in Tables III and IV. As discussed in the following, these results play a key role when interpreting the statistical outcomes obtained from the evaluation of NUCAPS-derived SIPs.

B. NUCAPS-Derived SIPs versus standard RAOBs

This section discusses the evaluation of the NUCAPS-derived SIPs relative to RAOB-derived SIPs. Over the tropics, only TPW, KI and GDI are evaluated since, by definition or by traditional use (e.g., KI), these parameters are judged useful for operational forecasting applications over this region. Relevant considerations carried out in this validation are: (1) The STD and BIAS are computed from the difference between

TABLE III

NUCAPS AVTP AND AVMP STATISTICS OVER MIDLATITUDES COMPUTED AT PRESSURE LEVELS GERMANE TO STABILITY INDEX COMPUTATION

Pressure Level (hPa)	AVTP				AVMP			
	Standard Deviation (K)	Bias (K)	Linear Correlation *r*	Number of Points	Standard Deviation (%)	Bias (%)	Linear Correlation *r*	Number of Points
500	1.190	0.636	0.978	11107	34.365	-12.155	0.820	11104
700	1.490	0.460	0.974	11122	28.013	-7.509	0.820	11122
850	1.893	-0.264	0.968	10649	25.633	-5.247	0.746	10633
950	2.855	-1.399	0.897	8885	22.489	-10.381	0.766	8611

TABLE IV

NUCAPS AVTP AND AVMP STATISTICS OVER THE TROPICS COMPUTED AT PRESSURE LEVELS GERMANE TO STABILITY INDEX COMPUTATION

Pressure Level (hPa)	AVTP				AVMP			
	Standard Deviation (K)	Bias (K)	Linear Correlation *r*	Number of Points	Standard Deviation (%)	Bias (%)	Linear Correlation *r*	Number of Points
500	1.360	0.256	0.945	4478	32.551	-17.834	0.864	4477
700	1.576	0.089	0.939	4491	32.670	-8.576	0.826	4491
850	2.009	0.517	0.948	4100	24.231	-11.714	0.843	4087
950	2.315	-0.389	0.912	2939	19.590	-5.533	0.871	2801

the values of the SIPs derived from NUCAPS and RAOBs; and (2) for comparison purposes, a least squares procedure was used to calculate the best-fit curve, assuming a 2nd degree polynomial of the form $y = a_0 + a_1x + a_2x^2$, between the pairs RAOBs and NUCAPS SIPs. It is important to notice that the NUCAPS and RAOBs datasets used in the validation of the NUCAPS SIPs are the same datasets used to compute the profile statistics presented in Section V-A.

1) TPW

As depicted in Fig. 5, the NUCAPS and RAOBs versions of TPW show high level of statistical agreement with remarkable values of linear correlation (above 0.87) over both regions. Another important result is the NUCAPS BIAS of around -2 mm over both regions, which implies a slight underestimation of NUCAPS TPW values in relation to RAOBs. This underestimation is shown graphically by the scatter diagrams in Fig. 5, in which most TPW points are below the reference "perfect-fit" line (in black), particularly for values above 15 mm. The analysis of histograms (figures not shown) indicates that the NUCAPS relative frequencies are around 11% and 8% below RAOBs frequencies for the class intervals above 25 mm over midlatitudes, and above 40 mm over the tropics, respectively. Overall, the scatter plots of Fig. 5, which show the entire collocation datasets used in the computation of the TPW statistics and contain a large dynamic range of observed TPW values ranging from about 5 mm (very dry) to around 70 mm (highly moist), indicate that the NUCAPS TPW has low bias associated with small values of RAOB TPW, and that those bias values become larger as the RAOB TPW values increase.

TPW is by definition the vertical integration of the water vapor content throughout the entire atmospheric column. In this context, the potential differences between NUCAPS and RAOBs moisture profiles found at few specific pressure levels impact less the performance of the NUCAPS TPW in comparison to what will be verified for the other SIs, which are highly dependent upon the thermodynamic information at specific levels.

The fact that NUCAPS TPW values agree closely with conventional RAOB counterparts over both regions and over a wide range of observed TPW values, going from a few mm to large amounts, indicates that the NUCAPS TPW product is well suited to be employed in the forecasting process. This is important because TPW is a widely used parameter to assess the potential for heavy precipitation (typically associated with plumes of elevated TPW values), which provides forecast guidance, for example, for the issuing of flash flood watches and warnings. However, users should consider that NUCAPS TPW magnitudes tend to be lower than their equivalent RAOBs versions, particularly for very high values of TPW.

2) SWI and LI

Due to the conceptual similarities between the SWI and LI, results derived from both indices are summarized in this subsection. The scatterplots presented in Fig. 6 indicate reasonably good values of linear correlation of about 0.64 and 0.70 for the LI and SWI, respectively. In the case of the STD, results show a value of 3.1°C for the SWI, and 3.9°C for the LI, revealing considerable variability of the SWI and LI values derived by NUCAPS with respect to the corresponding indices computed from conventional RAOBs. As the RAOBs SWI and LI values approach to zero, their NUCAPS counterparts tend to have larger magnitudes (note that most points are above the reference "perfect-fit" line in this case). Histograms (figures not shown) indicate that the relative frequencies of the NUCAPS SWI and LI are about 6.5% and 10.5%, respectively, lower than the RAOBs SWI and LI frequencies for the class interval below 0.0°C. Given that decreasing SWI and LI values are associated with increasing instability, previous results suggest that NUCAPS SWI and LI exhibit certain tendency for underestimation of unstable atmospheric conditions with respect to RAOBs. This is of special relevance

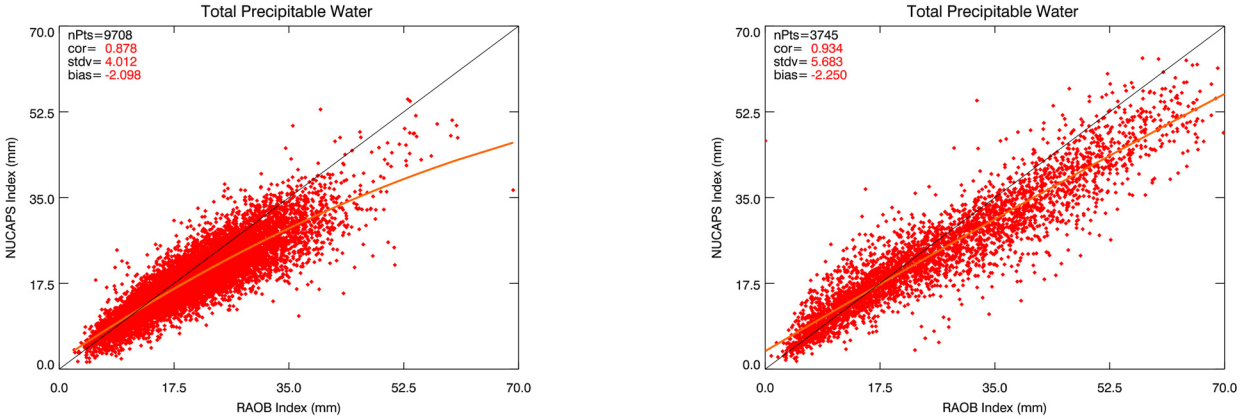

(a) (b)

Fig. 5. Scatterplots of conventional RAOBs versus NUCAPS TPW for: (a) midlatitudes and (b) tropics.

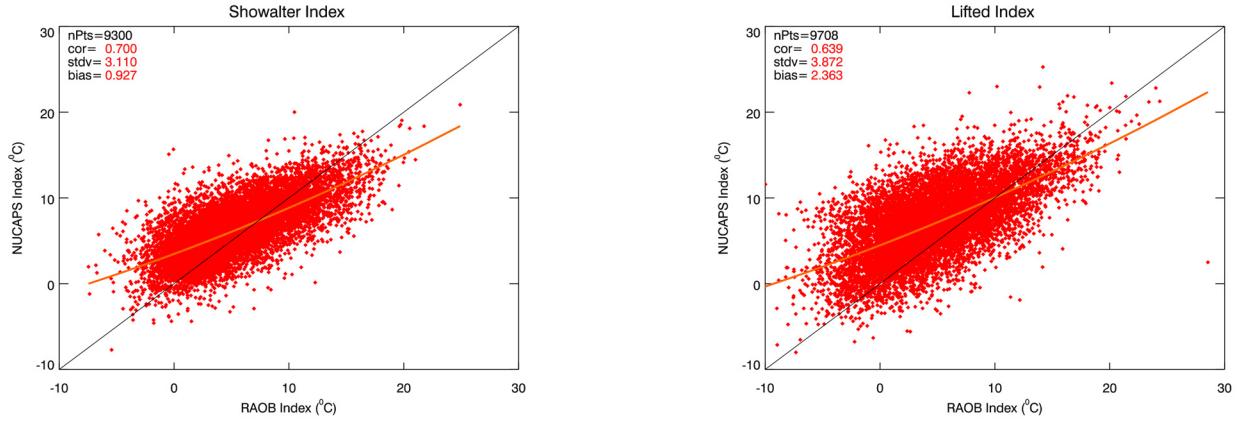

(a) (b)

Fig. 6. Scatterplots of conventional RAOBs versus NUCAPS versions of SWI (a) and LI (b) for midlatitudes.

given that the LI is among the most commonly used stability products on the operational forecasting routine.

By definition, the SWI and LI involve the lifting of low-level air parcels to the 500-hPa level, where parcel temperatures are compared with the ambient temperature at that level. An unsaturated air parcel undergoes a dry adiabatic ascent, but if it becomes saturated (the pressure level where saturation first occurs defines the LCL), its subsequent ascent will follow a pseudo adiabatic process. In this respect, the NUCAPS derived thermodynamic characteristics of the low-level parcel, as well as the ambient temperature at 500 hPa are determinant to the quality of the resulting SWI and LI indices. Referring back to Section V-A, the NUCAPS AVTPs are cold biased (i.e., NUCAPS AVTPs tend to be on average lower than RAOBs temperatures) at the lowest levels and slightly warm biased in the middle troposphere at midlatitudes (see Fig. 2 and Table III). Moreover, NUCAPS AVMPs are slightly dry biased below 300 hPa (see Fig. 3 and Table III). Considering the thermodynamics theory of the lifting process, and assuming dewpoint depressions that allow low-level air parcels reach the LCL, with the water vapor content (i.e., dewpoint) held constant, colder low-level air parcels in adiabatic ascent result in lower 500-hPa parcel temperatures. With the temperature held constant, drier low-level air parcels in adiabatic ascent also result in lower 500-hPa parcel temperatures stemmed from the reduced contribution of the latent heating. As part of the LI computation, temperature and mixing ratio from atmospheric levels within the lowest 100 hPa were averaged to define the mean parcel (MP) characteristics. In this case, the systematic errors (cold and dry biases) of the NUCAPS thermodynamics profiles at the lower levels are responsible for generating 500-hPa parcel temperatures colder than those produced by RAOBs. Mathematically speaking, these factors contribute to diminish the value of the second term of (5). In addition, the 500-hPa NUCAPS warm BIAS of around 0.6 K (see Table III) signifies that the NUCAPS-derived 500-hPa ambient temperatures tend to be slightly higher than the corresponding RAOBs-derived temperatures, which contributes to increase the value of the first term of (5). Thus, NUCAPS tends to produce less buoyant parcels, which yields more positive (or less negative) LIs. Similar considerations apply for the interpretation of the results of NUCAPS SWI. In this case, the NUCAPS derived SWI shows better agreement with respect to the RAOBs values because the hypothetical parcel assumes thermal and moisture characteristics of the 850-hPa level. For this specific level, the NUCAPS temperature and moisture biases are low (about −0.26 K for temperature and −5.25% for water vapor, as shown in Table III), introducing smaller errors into the NUCAPS SWI computation in comparison with the NUCAPS

LI case. Therefore, the NUCAPS LI is more affected by the low-level biases of the NUCAPS AVTPs and AVMPs.

In Section V-A, it was verified that the NUCAPS MP temperature is in better agreement with RAOBs than the NUCAPS MP dewpoint. Then it is now important to consider the implications of these results on the NUCAPS LI. First, it can be noted from Fig. 4(b) that a detrimental effect on the general statistics of the NUCAPS dewpoint arises from the larger dispersion of points located at the extreme left portion of the scatterplot, which corresponds to very cold and dry atmospheric conditions. This suggests that the NUCAPS skill in deriving the MP dewpoint is reduced under such extreme atmospheric conditions. Nevertheless, these situations are not the focus of attention for forecasters interested in diagnosing favorable atmospheric conditions for convective development. On the other hand, under warm humid atmospheric conditions, the lower performance of NUCAPS dewpoints, in comparison to temperatures, is expected to have larger influence on the NUCAPS skill in computing the LI, since the temperature of the lifting parcel is more sensitive to dewpoints than temperatures [49]. The statistical results presented here enable us to understand the behavior of the NUCAPS LI and SWI relative to their conventional RAOBs counterparts. Previous discussion had recognized that those results are affected by the intrinsic errors found in the comparison against RAOBs. This aspect will become more evident when comparisons against SIPs derived from synchronized reference/dedicated RAOBs are presented in Section V-C.

3) KI

Figs. 7(a) and 7(c) report the performance of the NUCAPS KI. High values of linear correlation, *r*, close to 0.8 and BIAS magnitudes of about 1ºC are found when comparing KI values estimated from NUCAPS and RAOBs. With respect to the STD, a larger value is seen over the tropics than over midlatitudes. In general, these results indicate that NUCAPS KI compares relatively well with respect to the RAOBs-derived values, while showing comparable performance over the tropics and midlatitudes. From Tables III and IV, as well as from the KI definition (Section III), it is possible to identify that the larger STD computed for NUCAPS KI over the tropics can be explained by the larger values of tropics temperature STD found at 850, 700, and 500 hPa. With respect to the impact of NUCAPS moisture profiles, the important levels to perform a similar analysis are 850 and 700 hPa, since moisture information from these levels are used for the KI computation. In this case, the major difference is found at the 700-hPa level, in which NUCAPS moisture STD is larger over the tropics than over midlatitudes. At the 850-hPa level, NUCAPS moisture STDs are equivalent at both regions.

The scatterplots also show how NUCAPS tends to produce lower KI values relative to RAOBs. This is observed for RAOBs KI approximately above10ºC, impacting particularly the generation of KI values above 30ºC, over the tropics, and above 25ºC, over midlatitudes, as depicted by the frequency distributions shown in Figs. 7(b) and 7(d). Referring back to the scatterplots, it can be verified that the RAOB/NUCAPS differences are larger for the RAOBs-defined values below −10ºC. According to the KI definition, all values below 10ºC fall within the category of very stable atmospheric conditions (not suitable for convective development). These situations are, in general, well resolved by NUCAPS, as shown by Figs. 7(b) and 7(d). The interval between 10 and 20ºC is also considered a range of stable conditions associated with very low probability of occurrence of thunderstorms. Figs. 7(b) and 7(d) show that, compared to RAOBs, NUCAPS KI tends to estimate more cases over the 10-20ºC interval, particularly over midlatitudes.

In short, our results indicate that NUCAPS and RAOBs KI values are highly correlated, which encourages operational applications of the NUCAPS KI. As seen above, NUCAPS KI is able to identify very stable conditions (defined by RAOBs KI below 10ºC), despite showing values that do not closely agree with RAOBs values. For RAOBs-defined KI values above 10ºC, the NUCAPS KI is capable of detecting the presence of instability, but with an observed tendency to derive underestimated KI values in relation to RAOBs as the instability increases. This is of special relevance during the analysis of the more unstable situations with higher likelihood of thunderstorms onset (KI above 30ºC). Under these circumstances, the use of the NUCAPS KI in the forecast process should consider the fact that the NUCAPS value would tend to be lower than the corresponding KI value derived from conventional RAOBs.

4) TT

NUCAPS TT exhibits a reasonably good level of agreement with RAOBs with a linear correlation of 0.690 (Fig. 8). As also shown, NUCAPS TT holds a low BIAS of -1.285ºC along with a STD of about 5.65ºC.

Like KI, TT depends on the temperature and humidity at specific atmospheric pressure levels. All of the NUCAPS/RAOBs differences in TT clearly reflect the performance of NUCAPS-derived AVTP/AVMP at those levels. According to TT formula (Section III), only the 500 and 850-hPa levels are used, and the temperature information represents the largest influence. Furthermore, the temperature at the 500-hPa level is subtracted twice in TT computation. From Table III, we had previously noted a warm BIAS of about 0.6 K at the 500-hPa level. Since NUCAPS-derived temperatures at 500 hPa tend to be, on average, larger than their RAOB counterparts, this term contributes to produce NUCAPS TT values lower than RAOBs. Given the lower magnitude of the negative temperature BIAS at 850 hPa (around -0.26 K), which is computed only once, the influence of the NUCAPS temperature at 500-hPa represents the major contribution to the overall negative BIAS found for NUCAPS TT.

The scatterplot also reveals that RAOBs TT values corresponding to very stable atmospheric conditions, in special below 20ºC, are associated with large RAOBs/NUCAPS discrepancies that are adversely influencing the statistics despite the few cases. The negative BIAS indicates an overall NUCAPS tendency for underestimation of the RAOBs TT values. This tendency is mainly driven by the NUCAPS TT values between 45 and 55ºC (Fig. 8(b)). Although underestimation in relation to conventional RAOBs is observed, NUCAPS TT shows capability to support

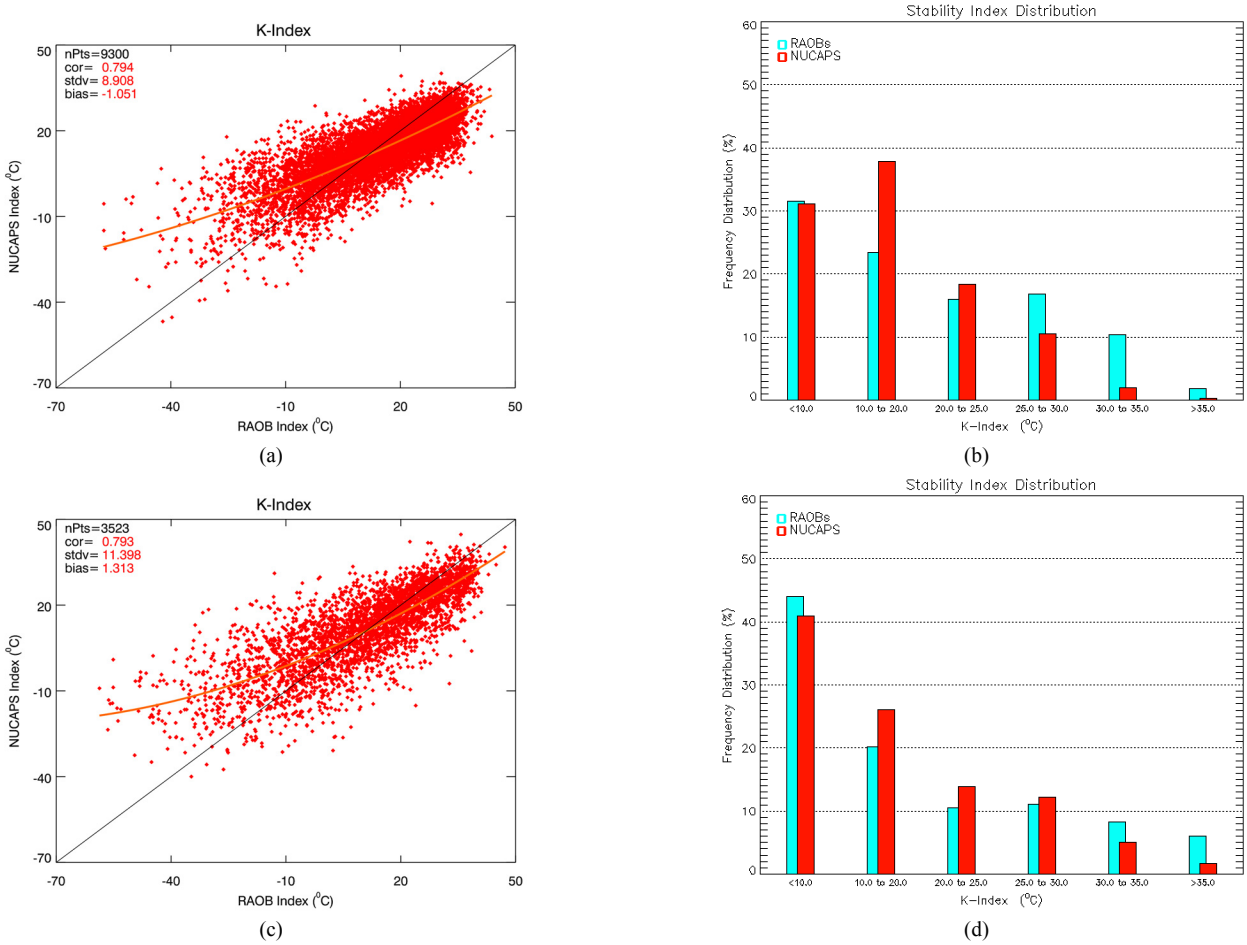

Fig. 7. Scatterplots of conventional RAOBs versus NUCAPS KI for: (a) midlatitudes and (c) tropics. Histograms of RAOBs/NUCAPS KI for: (b) midlatitudes and (d) tropics.

forecasting applications, as further discussed in Section VI-A.

5) GDI

Fig. 9(a) shows a high correlation of approximately 0.78 when NUCAPS GDI is compared against their corresponding RAOBs values. The statistical results also include STD of about 12 and BIAS of about −3.54. The negative BIAS indicates that NUCAPS GDI in general underestimates RAOBs GDI, which is particularly true for RAOBs GDI values above 10. This tendency becomes more evident for the highest GDI values, in which NUCAPS GDI potential for resolving the most intense cases of tropical convective instability (GDI > 35) seems somewhat restricted (see Fig. 9(b)).

The GDI is calculated with temperatures and mixing ratios at 950, 850, 700 and 500 hPa. The thermodynamic properties at those levels are used during several stages of the multi-step calculation of GDI (see [40]). More specifically, the calculation of GDI is highly dependent on the equivalent potential temperature (θ_e), an important thermodynamic parameter that incorporates both temperature and moisture content (mixing ratio) on its formulation. The θ_e is defined as the temperature an air parcel would have if lifted dry adiabatically to its LCL, and then pseudo adiabatically (with respect to water saturation) to zero pressure, condensing all its water vapor, dropping out condensed water, and finally brought down dry adiabatically to 1000 hPa [44], [50]. Conceptually, the variation of θ_e with height is a criterion to assess the convective (or potential) stability of the atmosphere [51]. Therefore, GDI requires the computation of θ_e profiles to diagnose (1) warm moist unstable atmospheric conditions, and (2) subsidence (trade wind) inversions (localizing the decrease in the moisture content of a column associated with the temperature inversion) [37]. As a result of the dependence of θ_e on temperature and humidity, the RAOB/NUCAPS differences in these parameters (as shown in Table IV) are affecting the accuracy of the NUCAPS θ_e, and consequently, of the NUCAPS GDI. Given the critical dependence of the final θ_e upon the latent heat released during the pseudo adiabatic ascent (used to warm the lifting air parcel), the magnitude of NUCAPS θ_e differences in relation to RAOBs must increase in warm humid atmospheric conditions. In this case, the drier NUCAPS-derived parcels (resulting from the NUCAPS water vapor negative biases found for the four levels used during GDI computation) produce lower θ_e values than the ones produced by RAOBs, and larger RAOB/NUCAPS θ_e differences in comparison with drier environments. On the contrary, in drier conditions, the contribution of the latent heat release to the θ_e is less important since air parcels contain less moisture. This means that under these conditions, the negative biases found for NUCAPS water vapor become a less significant source of error for the final

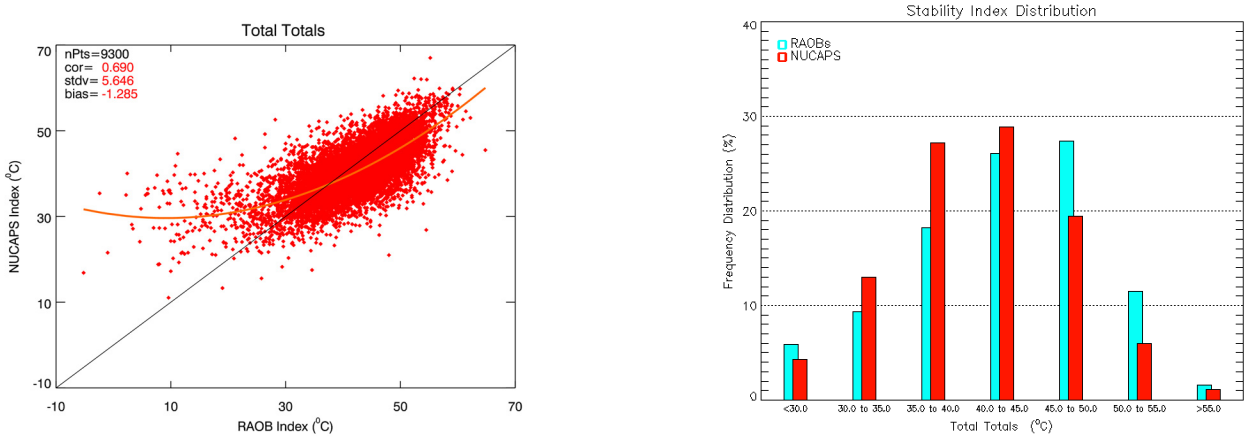

(a) (b)

Fig. 8. (a) Scatterplot of conventional RAOBs versus NUCAPS versions of TT for midlatitudes. (b) Histogram of RAOBs/NUCAPS TT for midlatitudes.

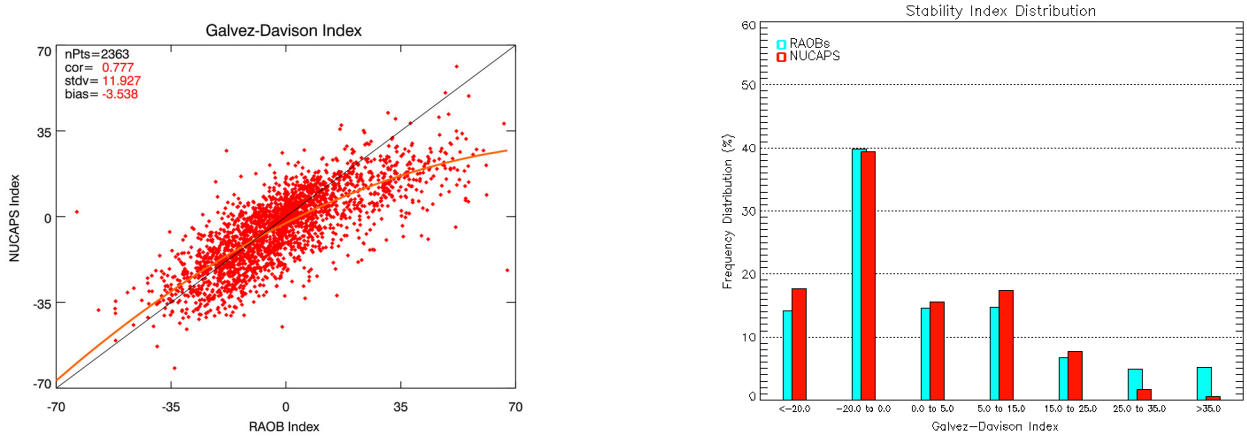

(a) (b)

Fig. 9. (a) Scatterplot of conventional RAOBs versus NUCAPS versions of GDI for the tropics. (b) Histogram of RAOBs/NUCAPS GDI for the tropics.

NUCAPS θ_e, resulting in smaller RAOB/NUCAPS differences. The previous discussion helps elucidate the behavior of GDI values higher than about 30 (RAOBs-defined), in which NUCAPS GDI tend to be underestimates of RAOBs GDI. According to its definition, GDI above 30 typically occurs in warm humid convectively unstable environments (free of inhibiting factors for convective weather, such as subsidence inversions and mid-levels ridges). Under such conditions, the comparisons against conventional RAOBs indicate that the applicability of NUCAPS GDI as an indicator of instability becomes considerably limited. To overcome this deficiency, we recommend the use of NUCAPS GDI in combination with other indices or parameters, like KI and TPW, as we have discussed and demonstrated later in Section VI-B using a case study of active convection associated with a tropical squall line. With this approach, we anticipate that NUCAPS GDI can help delineate the areas favorable for the development of tropical convection. In fact, the use of a combination of RAOB-derived stability parameters is a standard forecasting practice among operational forecasters since, by definition, no single index would be able to fully characterize the convective potential of the atmosphere. This same approach should then be employed when utilizing NUCAPS-derived stability parameters in the forecasting routine. Moreover, forecasters should take advantage of some NUCAPS properties not hold by RAOBs. For example, NUCAPS has the capability of generating fields of atmospheric stability, which is not feasible with RAOBs. Therefore, it is recommended to use spatial maps of NUCAPS SIPs to distinguish unstable and stable air masses within a large-scale context (from the upper bound of the mesoscale to the synoptic scale). This will be shown in the cases studies of Section VI.

The results from the overall statistical analyses of the NUCAPS SIPs highlight the importance of improving the NUCAPS humidity, particularly within the boundary layer. An improvement of the retrieval first guess is expected to contribute to this purpose, since the NUCAPS humidity highly relies on the first guess in the boundary layer due to the insufficient information content found in the satellite observations to adequately resolve the vertical fine structure of the water vapor. A further optimization of the water vapor channels used in the algorithm (particularly those with high sensitivity to water vapor variations near the surface) is another aspect that should also be investigated, in order to increase the retrieval sensitivity to extremely moist conditions and therefore increase the current water vapor dynamic range. Another alternative resides on the improvements in the surface emissivity, which are expected to enhance the performance of the NUCAPS soundings in the boundary layer.

TABLE V
PERFORMANCE SUMMARY OF NUCAPS SIPS COMPUTED AGAINST REFERENCE/DEDICATED (REF/DED) AND CONVENTIONAL (CONV) RAOBS[a]

SIP	Standard Deviation (ref/ded)	Standard Deviation (conv)	Bias (ref/ded)	Bias (conv)	Linear Correlation *r* (ref/ded)	Linear Correlation *r* (conv)	Number of Points (ref/ded)	Number of Points (conv)
TPW	3.216	4.012	-0.326	-2.098	0.959	0.878	620	9708
LI	3.486	3.872	0.658	2.363	0.813	0.639	620	9708
SWI	2.801	3.110	0.605	0.927	0.828	0.700	610	9300
KI	9.045	8.908	1.311	-1.051	0.849	0.794	610	9300
TT	5.775	5.643	-0.393	-1.285	0.745	0.690	610	9300

[a]STD and BIAS units: TPW in mm; remaining SIPs in ºC.

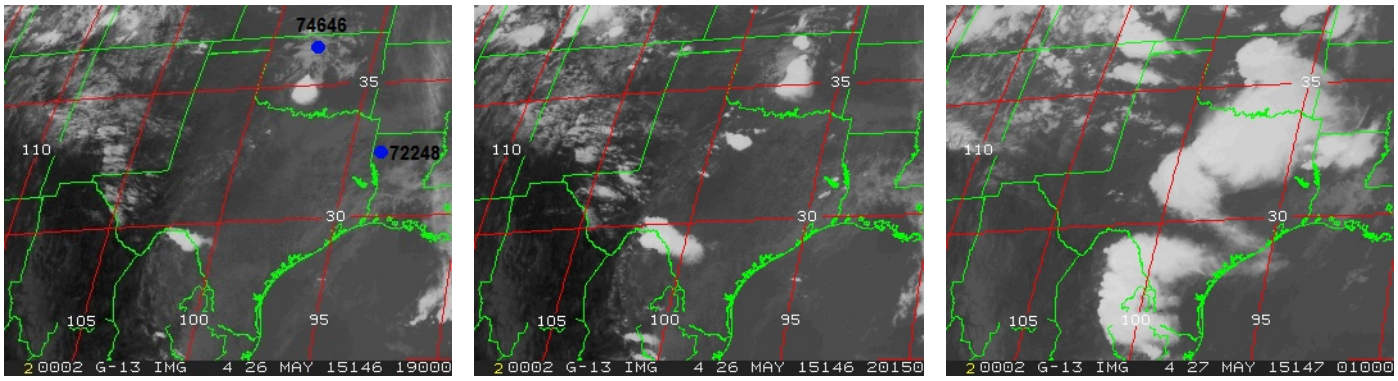

(a) (b) (c)

Fig. 10. GOES-13 IR imagery at 1900 UTC (a), 2015 UTC (b) 26 May 2015, and 0100 UTC (c) 27 May 2015. The dots identify the location of the Lamont, OK (WMO ID: 74646) and Shreveport, LA (WMO ID: 72248) radiosonde stations. (Courtesy of the NOAA Comprehensive Large Array-data Stewardship System - CLASS. Available online at http://www.class.ncdc.noaa.gov/saa/products/welcome).

C. NUCAPS-Derived SIPs versus Reference/Dedicate RAOBs and Summary Comparison

Dedicated/reference RAOBs constitute a supplemental data set with optimum accuracy and quality of the radiosonde sensors and synchronized with satellite observations. For this reason, comparisons of NUCAPS-derived SIPs versus those derived from dedicated/reference radiosondes are included to complement the comparisons against conventional RAOBs. Table V summarizes the statistical scores (midlatitudes) for the assessment based on dedicated/reference RAOBs along with the results from the analysis based on conventional RAOBs presented above. As shown in Table V, all linear correlations consistently increased when NUCAPS-derived SIPs are compared against SIPs produced from reference/dedicated RAOBs. The major change occurred for the LI, in which the linear correlation increased from about 0.64 to approximately 0.81. Moreover, there was an overall reduction in the NUCAPS statistical errors (systematic and random) when reference/dedicated RAOBs are used during the NUCAPS SIPs assessment. This overall amelioration can be explained by the reduction on the satellite-RAOBs collocation errors as well as the better error characterization and optimum accuracy of the reference/dedicated radiosonde sensors [42].

Regarding the application of the NUCAPS stability products in the operational meteorology, it is relevant to analyze the STDs summarized in Table V that provide an indication of the overall variability around the mean differences between the NUCAPS and RAOBs products. Remember that these mean differences correspond to the BIAS. For instance, the STD computed from the reference/dedicated RAOBs for the NUCAPS KI is approximately 9ºC. In general, forecasters use KI values exceeding 30ºC as the threshold criteria to indicate a strong potential for the occurrence of thunderstorms. Hence, a RAOBs KI of 30ºC can be associated with NUCAPS KI values ranging approximately from 22ºC to 40ºC. The same reasoning applies to the other SIs (as well as for STDs computed from conventional RAOBs). The STDs shown in Table V can then be used to define the interval of confidence of the NUCAPS SIPs, and it is recommended to display the value of the STDs of the NUCAPS SIPs along with their absolute values. This means that forecasters should not initially disregard NUCAPS SIs values ranging between their theoretical threshold indicative of high convective potential (e.g., 30ºC for KI, etc.) and the lower bound given by their STDs (e.g., 22ºC for KI, etc.) without a further scrutiny. The NUCAPS stability products are not intended to be used as stand-alone tools, instead they are expected to be used as a well-characterized air stability information oriented to supplement conventional forecasting data sources and to improve their temporal and spatial coverage. In this respect, it is expected that the NUCAPS SIPs reinforce the final forecasting decision-making process by contributing to the development of a robust weather forecasting dataset.

VI. NUCAPS APPLICATIONS TO CASE STUDIES

In consideration of the fact that previous statistical analyses do not provide a thorough understanding of the applicability of NUCAPS-derived SIPs to short-term forecasting, two case

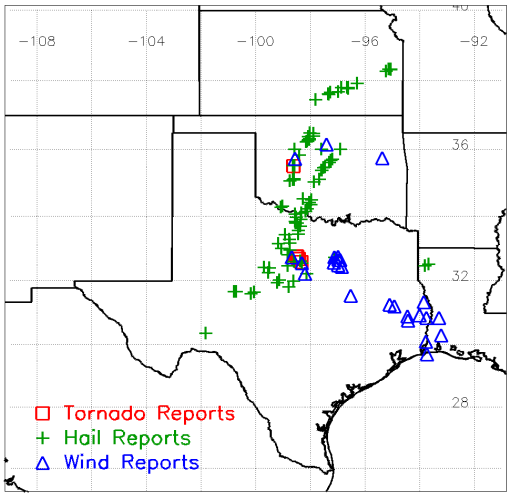

Fig. 11. The reported high winds, hail and tornado locations between 1200 UTC 26 May and 1159 UTC 27 May 2015 (map based on reports received by the NOAA/Storm Prediction Center (SPC) available online at www.spc.noaa.gov/climo/reports/150526_rpts.html).

studies involving typical scenarios of convective weather development are presented. The meteorological events analyzed here occurred in the North America midlatitudes and in the tropical region of the South America, highlighting the adaptability of NUCAPS SIPs to very distinct climatic regimes.

Recall that the SNPP is a sun-synchronous satellite with ascending and descending orbits crossing the equator at approximately 1330 and 0130 LT, respectively. Thus, the satellite passage times are important factors to consider for weather forecasting applications of NUCAPS SIPs at any location. For example, the geographical domain of the first case study is located over the continental U.S (CONUS). In this case, the SNPP overpasses this region from the east to the west direction during the ascending mode between about 1700 and 2300 UTC. The second study area is located in Brazil, where the SNPP passage times (ascending mode) are between approximately 1600 and 1900 UTC.

A. 26 May 2015 Great Plains Severe Thunderstorms Outbreak

In the early afternoon of 26 May 2015, isolated thunderstorms started developing along a dry line over Texas, as well as ahead of a frontal boundary over Oklahoma (the reader can refer to [52]–[54] for the Weather Prediction Center (WPC) Surface Analysis, which shows the weather systems and meteorological surface observations over the CONUS at 1800 UTC 26 May 2015, and the legends of the symbols used in this type of meteorological chart). Southerly low-level winds provided the inflow of warm moist air from the Gulf of Mexico into the Texas-Oklahoma region. This mechanism in conjunction with the destabilizing effect of the daytime heating favored the establishment of steep vertical lapse rates. At 1800 UTC, dewpoint temperatures around 17ºC were observed over Oklahoma and northwestern Texas (ahead of the dry line), increasing to values near 24ºC in the southernmost locations of Texas [52]. The range of dewpoint temperatures observed over the case study area reflects a very humid preconvective environment. The SNPP passed over the

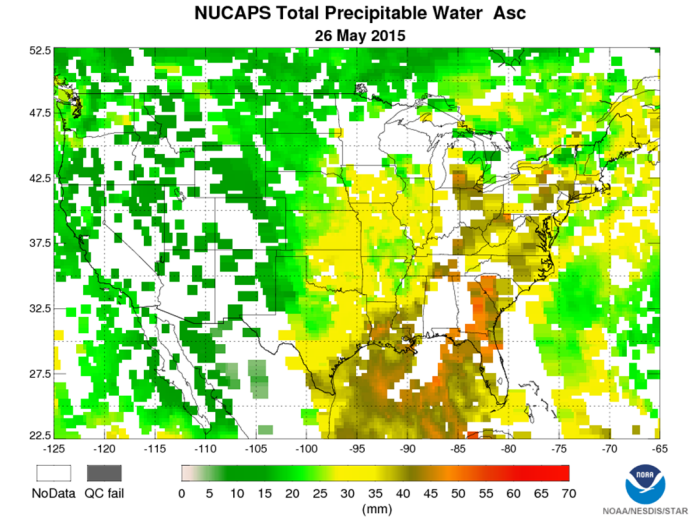

(a)

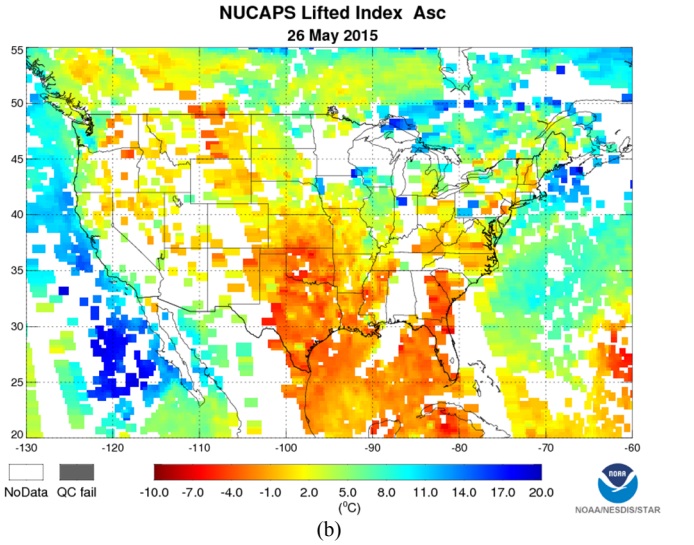

(b)

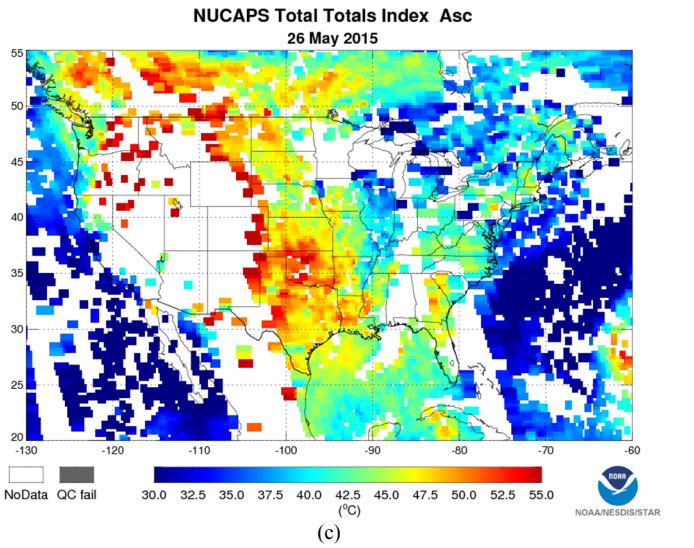

(c)

Fig. 12. TPW (a), LI (b) and TT (c) fields derived by NUCAPS for 26 May 2015 (SNPP ascending passage). TT values are not plotted in high-elevation regions where the TT is undefined. Note that SIPs values are not plotted in areas where the NUCAPS algorithm failed (these areas should be distinguished from the satellite orbital gaps). The start and end times (UTC) of the granules corresponding to the three main satellite swaths shown are: 17h:28min:33s−17h:40min:15s (right-swath), 19h:09min:21s−19h:21min:35s (center-swath), 20h:51min:13s−21h:01min:51s (left-swath).

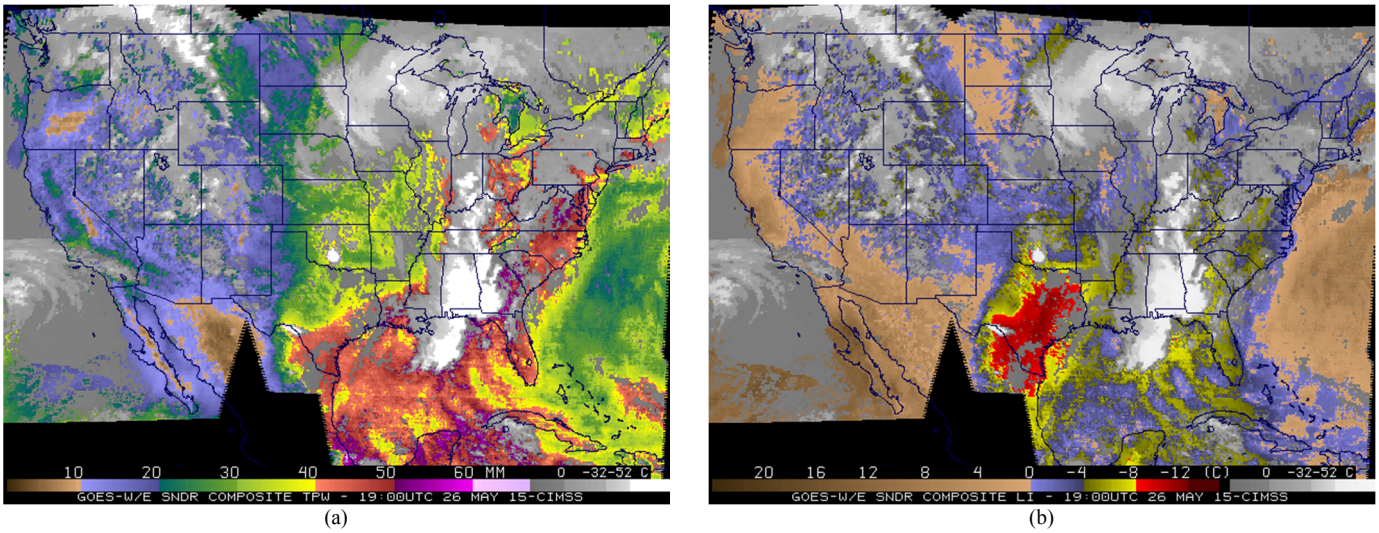

(a) (b)

Fig. 13. GOES sounder (a) TPW and (b) LI DPI products at 1900 UTC 26 May 2015. The maps are composites of GOES-13 (East) and GOES-15 (West) sounders data. (Courtesy of the SSEC/University of Wiscosin-Madison. Available online at http://cimss.ssec.wisc.edu/goes/rt/).

region (ascending mode) at about 1915 UTC. Fig. 10(a) depicts the GOES-13 IR image at 1900 UTC, in which few convective systems are visible over the south zones of both states. However, six hours later, further development into significant clusters of strong to severe thunderstorms occurred (Fig. 10(c)), resulting in numerous reports of hail and damaging winds, and a few tornadoes (Fig. 11).

Fig. 12(a) displays the NUCAPS TPW-derived field (SNPP ascending passage) on 26 May 2015. Despite limitations in areas under cloudy and precipitating conditions, NUCAPS provides useful indication of the regions within the domain with the largest TPW amounts. Over the case study area, NUCAPS indicates large TPW values (in excess of about 25 mm) over nearly all Oklahoma and most of Texas. An important meteorological feature revealed by the NUCAPS TPW map is the presence of a horizontal moisture gradient over the northwestern Texas. This moisture contrast is associated with the presence of the dry line, defined as a sharp mesoscale boundary between the moist air from the Gulf of Mexico and the drier continental air mass (from northern Mexico and southwestern US) behind it. This phenomenon, which occurs frequently during the Spring and early Summer over the case study region, is of great interest for forecasters, since it provides an initiating mechanism for deep convective storms [55]–[57]. In this sense, this case effectively exemplifies the capability of the NUCAPS TPW product to assist forecasters in the process of identification of spatial boundaries of moisture, which play a critical role in the initiation of convection.

Figs. 12(b) and 12(c) show the LI and TT fields, respectively, derived from NUCAPS, which reveal high potential for severe storm formation over Oklahoma/Texas. The unstable atmospheric conditions are given by negative values of the LI over most Texas and Oklahoma and the large positive values of TT. Note that some areas exhibit SI values related to very unstable conditions such as LI lower than -4ºC and TT larger than 50ºC. Of special interest is the fact that these areas associated with very unstable SI values (more evident for TT) occur approximately along a line stretching from southwestern Texas into the central portion of Oklahoma. This line is in very good spatial match with respect to the areas where the first thunderstorms developed (Figs. 10(a) and (b)).

NUCAPS TPW and LI are also compared with equivalent GOES Sounder derived product image (DPI) products (Figs. 13(a) and (b)) generated by the Space Science and Engineering Center (SSEC) at the University of Wisconsin-Madison (TT is not evaluated since this SI is not among the suite of GOES DPI products). The GOES DPI products were generated from temperature and moisture profiles derived from the clear-sky physical retrieval algorithm described in [9]. NUCAPS TPW (Fig. 12(a)) and GOES DPI TPW (Fig. 13(a)) are in very good agreement, although the GOES product indicates larger TPW values between 40 and 50 mm

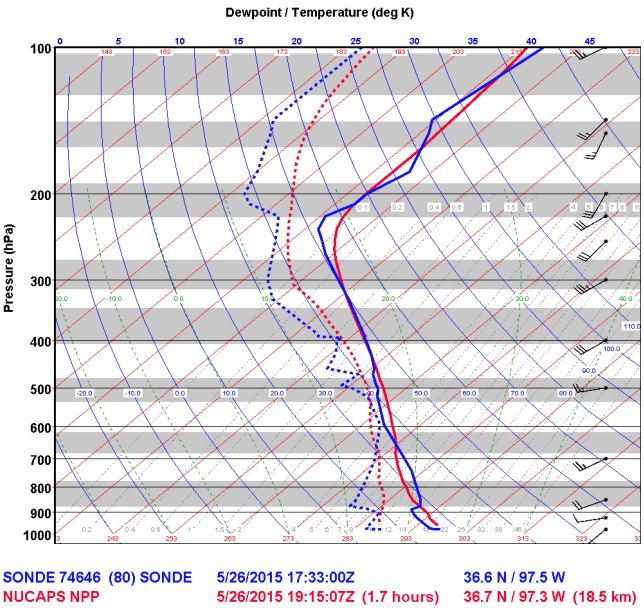

Fig. 14. Temperature (solid) and dewpoint temperature (dashed) profiles from NUCAPS (red) and RAOB (blue) over Lamont, Oklahoma, on 26 May 2015. Times (in UTC) and location of sounding observations are indicated in the bottom legend. Time and distance differences between the RAOB and SNPP overpass are found in parenthesis.

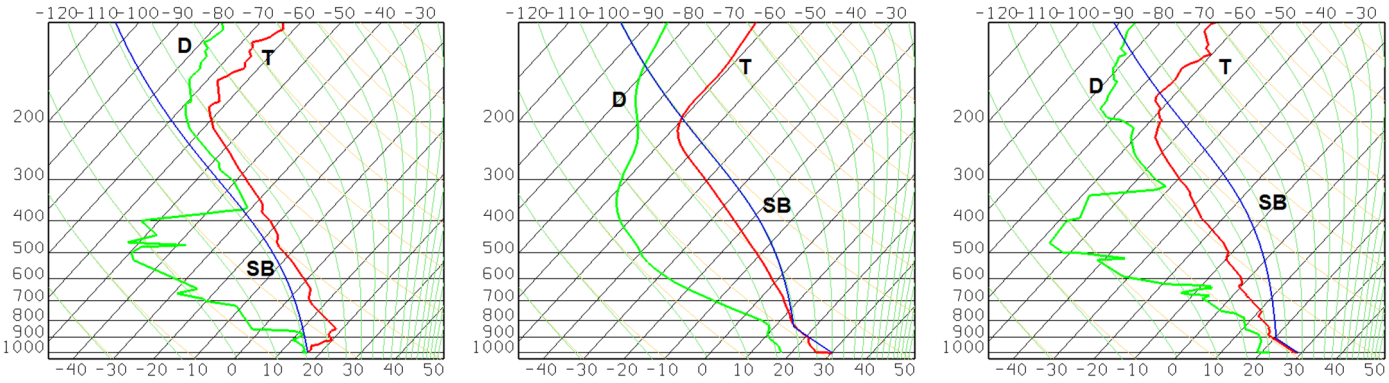

Fig. 15. RAOBs over Shreveport, Louisiana at 1200 UTC 26 May 2015 (a), and 0000 UTC 27 May 2015 (c). NUCAPS thermodynamic profile over Shreveport, Louisiana at 1913 UTC 26 May 2015 (b). The vertical axis is labeled in units of pressure (hPa) and the horizontal axis is labeled in units of temperature (ºC). Temperature is represented by the curve labeled as T, dewpoint temperature is represented by the curve labeled as D, and the curve labeled as SB denotes the surface-based parcel trajectory.

TABLE VI
SIPS COMPUTED USING RAOBS FROM LAMONT, OK (36.62°N, 97.48°W) AND SHREVEPORT, LA (32.46°N, 93.78°W) STATIONS, AND NUCAPS RETRIEVALS FOR THE CLOSEST FIELD OF REGARD (FOR) TO EACH LOCATION. DISTANCE BETWEEN RAOB LAUNCH AND NUCAPS FOR IS PROVIDED IN KILOMETERS.

Station (WMO Identifier)	Day/Time (UTC)	Profile Type	TPW (mm)	LI (ºC)	TT (ºC)
Lamont, OK (74646)	26 May 2015 1200	RAOB	25.20	1.81	46.80
	26 May 2015 1800	RAOB	28.30	-1.36	49.60
	26 May 2015 1915 (18.5 km)	NUCAPS	30.71	-2.67	50.72
	27 May 2015 0000	RAOB	30.90	-5.42	52.80
Shreveport, LA (72248)	26 May 2015 1200	RAOB	21.30	2.54	39.20
	26 May 2015 1913 (10.3 km)	NUCAPS	27.09	-2.76	47.85
	27 May 2015 0000	RAOB	33.57	-5.41	49.63

over the south portion of Texas whereas NUCAPS TPW values are between 30 and 45 mm in the same area. With respect to the LI (Figs. 12(b) and 13(b)), both products are in overall good spatial agreement regarding the location of stable and unstable zones, although NUCAPS is effective in highlighting the linear unstable signature associated with thunderstorm genesis. A notable difference is seen over the eastern and southern portions of Texas where the GOES DPI LI indicates extreme instability with values lower than -8 ºC whereas NUCAPS LI values are within the range of -2 to -6 ºC. Nevertheless, from the high correspondence between the linear unstable signature shown by NUCAPS LI and the locations where high winds, large hail, and tornadoes were reported (Fig. 11), NUCAPS provided a more specific indication of the areas with higher likelihood for thunderstorm genesis in the case study domain. In addition, the GOES DPI LI is not able to detect the highly unstable conditions over Oklahoma as successfully detected by NUCAPS and confirmed by the storm reports presented in Fig. 11. The main reason is the limitation of GOES to operate in cloudy conditions. The GOES stability products have been important ancillary tools to monitor atmospheric stability conditions with high temporal resolution for over two decades [6]. In this perspective, our work has demonstrated that the stability parameters derived from NUCAPS constitute a high-quality alternative to the GOES legacy sounding products. Furthermore, NUCAPS SNPP CrIS/ATMS has additional advantages over narrowband sensors (e.g., GOES ABI) [18], including global coverage, soundings available under cloudy conditions, and the capability to produce retrieved profiles with improved accuracy and higher vertical resolution.

Unlike the GOES physical retrieval algorithm, which requires numerical weather prediction (NWP) forecasts as a component of the predictors for the linear regression scheme that generates its first-guess [9], [11] (surface temperature and moisture observations are also used), NUCAPS first-guess profiles are obtained from the IR and MW radiances. More specifically, NWP model outputs are not part of the input ancillary data needed to process the algorithm, except for the surface pressure obtained from the GFS model. In this sense, the NUCAPS soundings are independent source of information, not affected by eventual biases present in the NWP models. This attribute can be valuable to forecasters, for example, to help assess the skill of the NWP output (e.g., a model-forecasted sounding), which could increase the confidence in the model or lead to the identification of disparity in the model solutions.

Fig. 14 depicts the skew-T plot of the 1800 UTC RAOB for the Lamont, OK sounding station (see location in Fig. 10(a)) and the NUCAPS sounding produced for the closest NUCAPS FOR to this location (SNPP ascending passage) on 26 May 2015. The existing temporal and spatial differences between those observations are 1.7 h and 18.5 km, respectively. It can be noted how NUCAPS is able to represent the overall thermal structure in agreement with the 1800 UTC RAOB. With respect to the dewpoint, NUCAPS also captures and follows the overall structure shown in the RAOB profile, but NUCAPS is not able to capture the rapid changes in the humidity profile as measured by the radiosonde. In the upper troposphere (above 400 hPa), the humidity differences are likely influenced by the fact that humidity measurements from operational radiosondes show dry biases, which are particularly larger for daytime observations [58], [59]. In the lower troposphere, NUCAPS does not capture a layer of drier

air centered approximately at 880 hPa. This feature is part of a capping inversion [60] identifiable in the RAOB profile as a shallow temperature inversion layer, in which temperature increases with height, between approximately 900 and 880 hPa. As seen in other satellite-derived soundings, this fine temperature structure was not resolved by NUCAPS due to its associated vertical resolution. Despite the fact that NUCAPS does not represent the vertical structure of the atmosphere with the finest details provided by the RAOBs, NUCAPS soundings contain sufficient information to allow the identification of unstable conditions in preconvective environments. This is seen in Table VI, which outlines TPW, LI and TT calculated using thermodynamic profiles from Lamont, OK and Shreveport, LA radiosonde stations and from the NUCAPS retrievals for the closest FOR to each location between 1200 UTC 26 May and 0000 UTC 27 May 2015. By showing increasing values of TPW and TT and lower values of LI, NUCAPS SIPs provide supplemental evidence on the evolution of statically unstable conditions at each site, which peaked later at 0000 UTC 27 May 2015. Note that Lamont, OK is among the few sounding stations performing 1800 UTC RAOBs. For the majority of U.S. sounding stations, the 1800 UTC RAOB is unavailable as in the case of the Shreveport, LA station. For this reason and the evident development of intense unstable conditions, we have used this latter station to show the benefit of NUCAPS soundings. For the Shreveport, LA station, the analysis of RAOBs profiles indicates a transition from a statically stable atmosphere at 1200 UTC (Fig. 15(a) - note the temperature inversion below 850 hPa and the negatively buoyant surface-based air parcel given by the parcel trajectory curve) to an unstable environment at 0000 UTC (Fig. 15(c)). Consistently, RAOB indices presented in Table VI indicate a marked decrease in the LI from about 2.5 to -5.4ºC, as well as a considerable increase in TT from 39.2 to 49.6ºC. The skew-T plot of the 1913 UTC NUCAPS profile (Fig. 15(b)) reveals a substantial positive area, defined as the region bounded by the ambient temperature profile and the parcel trajectory curve, from the LFC (located around 820 hPa in this case) to the equilibrium level (EL) (about 195 hPa). Note that the positive area is proportional to the Convective Available Potential Energy (CAPE), which is the vertical integration of the parcel buoyant energy (see [51] for a detailed definition). Above the LFC, the air parcel temperature exceeds the ambient temperature up to the EL, which generates positive buoyant energy that favors the upward vertical displacement of the parcel. This process had an important role in this meteorological event, providing the favorable environment for the vigorous convective overturning observed.

B. 04 June 2015 Northern Coast of Brazil Squall Line

The second convective event seeks to emphasize the usefulness of NUCAPS stability products over the tropics, represented here by the northern coast of Brazil (NCB). Fig. 16(a) shows the GOES-13 IR image for 04 June 2015 at 1615 UTC (1315 LT), the approximate time of the SNPP ascending passage over the focus region. In this case, few convective clouds were visible over the NCB at that time, however NUCAPS stability products displayed in Fig. 17 highlight the

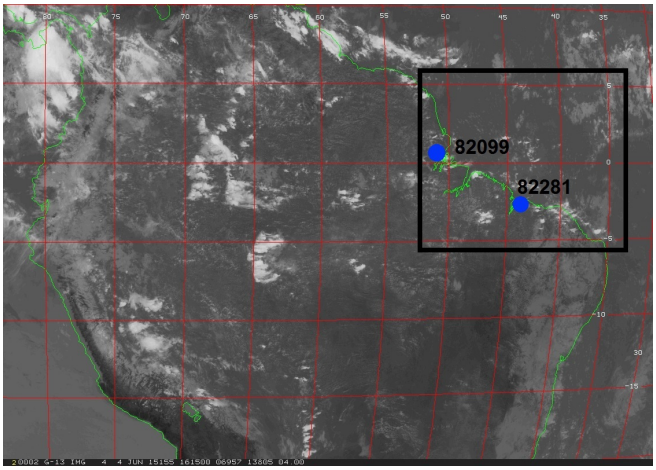

(a)

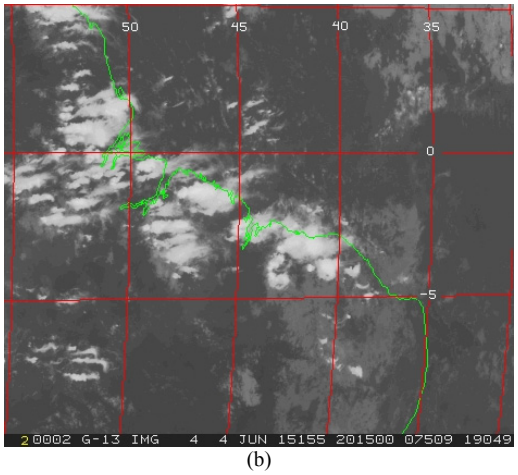

(b)

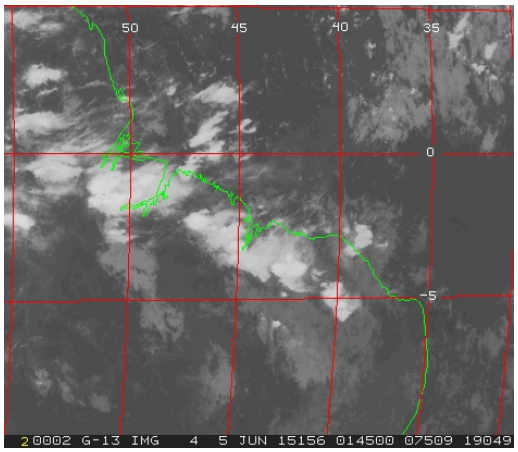

(c)

Fig. 16. GOES-13 IR imagery at (a) 1615 UTC 04 June 2015, (b) 2015 UTC 04 June 2015 and (c) 0145 UTC 05 June 2015. The black rectangle on the top panel highlights the NCB region. The dots identify the location of the Sao Luiz (WMO ID: 82281) and Macapa (WMO ID: 82099) radiosonde stations. (Courtesy of the NOAA Comprehensive Large Array-data Stewardship System - CLASS. Available online at http://www.class.ncdc.noaa.gov/saa/products/welcome.)

existence of strong potential for convective development over the study domain. Note how the values of NUCAPS GDI, KI and TPW noticeably increase towards the NCB, contrasting to their lower values (indicative of more stable and drier conditions) in the central and southern Brazil. During the following hours, an increasing number of convective cells

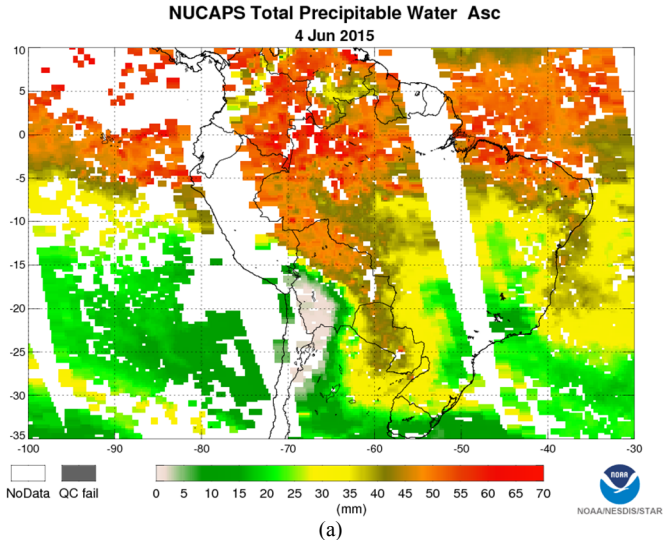

(a)

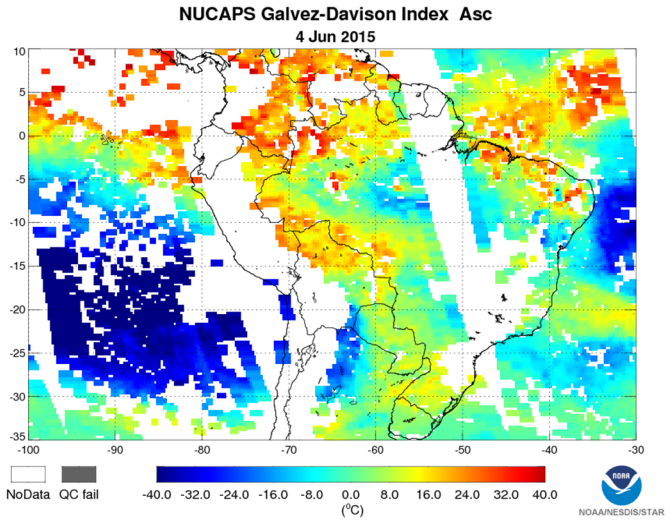

(b)

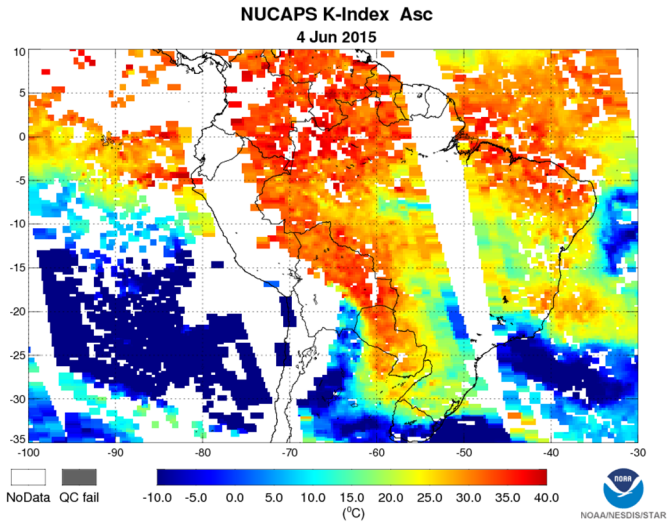

(c)

Fig. 17. TPW (a), GDI (b) and KI (c) fields derived by NUCAPS for 04 June 2015 (SNPP ascending passage). High-elevated areas where KI and GDI are undefined appear as blank. Note that areas where the NUCAPS algorithm failed are also shown as blank (they should be distinguished from the satellite orbital gaps). The start and end times (UTC) of the granules corresponding to the three main satellite swaths shown are: 16h:03min:05s−16h:16min:55s (right-swath), 17h:43min:53s−17h:58min:15s (center-swath), 19h:25min:13s−19h:39min:35s (left-swath).

TABLE VII
SIPs COMPUTED USING RAOBs FROM SAO LUIS, BRAZIL (2.60°S, 44.23°W) AND MACAPA, BRAZIL (0.05°N, 51.07°W) STATIONS, AND NUCAPS RETRIEVALS FOR THE CLOSEST FIELD OF REGARD (FOR) TO EACH LOCATION. DISTANCE BETWEEN RAOB LAUNCH AND NUCAPS FOR IS PROVIDED IN KILOMETERS.

Station (WMO Identifier)	Day/Time (UTC)	Profile Type	TPW (mm)	KI (ºC)	GDI
Sao Luiz (82281)	04 June 2015 1200	RAOB	48.52	29.10	24.32
	04 June 2015 1612 (26.2 km)	NUCAPS	52.86	33.50	17.18
	05 June 2015 0000	RAOB	54.00	34.10	26.80
Macapa (82099)	04 June 2015 1200	RAOB	51.34	35.50	20.10
	04 June 2015 1613 (81.4 km)	NUCAPS	52.73	33.21	13.37
	05 June 2015 0000[a]	RAOB	-	-	-

[a]Sounding not available.

developed along the coast, as shown by the GOES-13 IR image at 2015 UTC (Fig. 16(b)). This pattern of coastal genesis of convection, commonly observed in this region, is induced by the sea-breeze convergence zone [61]. As the small clusters of thunderstorms progressively merge into larger clusters, the sea-breeze induced convection frequently results in mesoscale to synoptic-scale squall lines that propagate inland parallel to the NCB, with larger frequency between April and August [62], [63]. In the present case study, the GOES-13 IR image at 0145 UTC 05 June 2015 (Fig. 16(c)) confirms the occurrence of a squall line over the NCB.

SIPs derived from RAOBs from two conventional sounding stations located in the NCB, namely Sao Luis and Macapa (see locations in Fig. 16 (a)), and their corresponding NUCAPS SIPs are presented in Table VII. Given that there is no 1800 UTC RAOB over the entire NCB, NUCAPS soundings produce useful updates on TPW and KI in relation to the previous 1200 UTC RAOB, confirming large availability of moisture and high potential for the occurrence of thunderstorms (KI $\geq$ 30ºC). On the other hand, the retrieval soundings produce a smaller GDI than the previous 1200 UTC RAOB at both locations, indicating that the NUCAPS GDI values are underestimated. This is in line with results reported in Section V-B, which showed that NUCAPS underestimates GDI values relative to RAOBs, particularly for those conditions where RAOBs GDI is greater than 10. Despite the underestimation in relation to standard RAOBs, Fig. 17(b) reveals that the NUCAPS GDI field captures and follows the spatial signature of tropical convection, showing potential as a supporting tool to evaluate the risk for thunderstorms and rain showers over large areas of the NCB.

Because the first convective clouds that give rise to the squall lines in the NCB are typically initiated around or after local noon [63], local forecasters can benefit from the use of NUCAPS stability products and vertical profiles derived from CrIS/ATMS measurements taken in the early afternoon. Like the U.S. case, rawinsonde launches in Brazil typically occur at 1200 and 0000 UTC (0900 and 2100 LT). Another aspect that adds substantial value for the use of NUCAPS products in that

region, as well as in many others worldwide regions, is the paucity of sounding observations. For instance, the entire NCB region comprises of only 5 operational aerological stations, not to mention that the entire country sums about 40 [64]. This means that large extents of South America would benefit from accurate satellite-based measurements to fill in the existing observational gap.

VII. Summary and concluding remarks

The current study has demonstrated the capability of NUCAPS CrIS/ATMS-derived SIPs in the assessment of atmospheric stability for the upper bound of the mesoscale to synoptic-scale applications. Objective comparisons against a large sample of ground-based RAOBs revealed that among all SIPs evaluated, NUCAPS TPW exhibited the highest level of statistical agreement with RAOBs counterparts over the tropics and midlatitudes. This is due to the fact that NUCAPS TPW is more favored, since it is less dependent on information at specific levels. The remaining SIPs exhibited favorable levels of agreement with their RAOBs-derived versions (linear correlations ranging from about 0.65 to 0.85). However, the statistical analyses indicated that NUCAPS stability parameters tend to underestimate RAOBs-derived values, particularly over the range associated with unstable atmospheric conditions. Main reasons behind this result are: the existence of a cold BIAS near the surface level below a warm BIAS layer (resulting in an increase in static stability of the atmosphere); and the dry BIAS present in whole tropospheric column (Section V-A). We included comparisons of NUCAPS-derived SIPs versus those derived from high-quality synchronized dedicated/reference radiosondes to complement the comparisons against conventional RAOBs. By consistently improving the statistics in relation to the assessment based on conventional RAOBs, results from the NUCAPS SIPs comparison against dedicated/reference RAOBs provide additional confidence in the capability of NUCAPS SIPs in diagnosing changes in the static stability of the atmosphere.

Unlike conventional RAOBs, NUCAPS offers the potential of generating horizontal fields of SIPs, giving forecasters the opportunity of analyzing the spatial structure of atmospheric stability. In this respect, the case studies underscore NUCAPS capability of generating reliable fields of atmospheric stability, identifying areas of: (1) high likelihood of thunderstorm development over distinct climatic and geographic regions a few hours before the intense convective cells are observed; and (2) stable atmospheric conditions, which are important to avoid false alarm situations.

Limitations on the accuracy of the NUCAPS retrievals are mainly caused by cloud contamination, and areas under precipitation, in which NUCAPS is unable to converge to a solution. Thus, where overcast and/or precipitating conditions exist within the NUCAPS FOR, NUCAPS thermodynamic profiles would be typically unavailable. On the other hand, when the profile is obtained over partly cloudy scenes, it is expected that the quality of the products be degraded in relation to cloud-free scenes due to errors introduced by the cloud clearing process. These errors, which affect the estimates of the clear column radiances, arise from sources such as errors in the estimated surface skin temperature, surface spectral emissivity, surface spectral bi-directional reflectance of solar radiation, and temperature and moisture profiles [23].

Of high value is the availability of the NUCAPS CrIS/ATMS AVTPs and AVMPs products in the early afternoon at many U.S. states, a critical time for the evaluation of the thermodynamic conditions of the atmosphere and its potential for the initiation of convection. In addition, the global limitations on the spatial RAOBs coverage should also be considered, since this is far from the ideal even in the U.S., where rawinsonde locations can be up to a few hundred kilometers apart. In this respect, we anticipate an additional benefit from the use of NUCAPS stability products in countries with limited infrastructure supporting meteorological observations, where RAOBs are extremely infrequent or even absent. Moreover, increased temporal coverage of NUCAPS soundings can be obtained through a constellation of platforms from the JPSS, Aqua EOS and MetOp missions due to the modular nature of the code.

The application of this work seeks to benefit current and potential users of the NUCAPS products. In this regard, NUCAPS soundings and stability products have been progressively implemented as part of the Advanced Weather Interactive Processing System (AWIPS) II, which is the operational display and analysis package in use by the National Weather Service (NWS). Our research aims at providing objective information about the performance of NUCAPS products, serving as a benchmark for the analysis performed by operational forecasters. It is expected that the results presented here help the user community to gain confidence and explore the application of the NUCAPS CrIS/ATMS soundings. It is through the consensus of the user community that NUCAPS is envisioned to gain value and applicability on the operational forecasting environment. A challenge in mesoscale forecasting is the anticipation of thunderstorm-generated hazardous winds, typically resulting from downbursts, defined in general as strong downdrafts that induce an outflow of potentially damaging winds on or near the ground [65]. Over the intermountain western U.S., downburst winds are the most prevalent of all severe convective weather types (i.e. hail, tornadoes, wind) and frequently impact aviation transportation. Future research will investigate the inclusion of a parameter that diagnoses convective downdraft instability, as exemplified in [66], in order to extend the utility of NUCAPS for severe thunderstorm monitoring and warning operations. Since CAPE is the most common parameter used by operational forecasters to evaluate severe thunderstorm likelihood, our future work will include a comprehensive evaluation of NUCAPS CAPE, in order to provide useful guidance about its potential applicability in the forecasting environment.

The operational application of the NUCAPS soundings and derived SIPs is not intended to replace RAOBs use. Satellite retrievals are unable to achieve the same vertical resolution of the radiosonde profiles, which means that the small-scale structures and changes in the thermodynamic profile are not resolved. Hence, it is recommended to make use of such products in combination with other observational data and analysis tools (e.g., numerical outputs, radar and satellite

imagery). Under this perspective, NUCAPS stability products are proposed to be complementary tools for nowcasting applications, particularly for the analysis of preconvective environments prior to the formation of cumulus clouds and deep convection.

This work represents the initial evaluation of the atmospheric stability products generated by observations from the JPSS series. All points addressed here aim at establishing a larger inquiry into the full capability of NUCAPS sounding and stability products.

ACKNOWLEDGMENT

The authors would like to thank Anthony Reale (NOAA/NESDIS) for providing the NPROVS collocation data set used in this work. The authors also thank Michel Davison and Jose M. Galvez (NOAA/NCEP/WPC) for sharing their valuable experience with the GDI, and three anonymous reviewers for their constructive comments and suggestions for this manuscript. The views, opinions, and findings contained in this paper are those of the authors and should not be construed as an official NOAA or U.S. Government position, policy, or decision.

REFERENCES

[1] M. D. Goldberg, H. Kilcoyne, H. Cikanek, and A. Mehta, "Joint Polar Satellite System: The United States next generation civilian polar-orbiting environmental satellite system," *J. Geo phys. Res. Atmos.*, vol. 118, no. 24, pp. 13463–13475, Dec. 2013. doi: 10.1002/2013JD020389.

[2] C. M. Hayden, "GOES-VAS simultaneous temperature–moisture retrieval algorithm," *J. Appl. Meteor.*, vol. 27, no. 6, pp. 705–733, Jun. 1988. doi: 10.1175/1520-0450(1988)027<0705:GVSTMR>2.0.CO;2.

[3] W. L. Smith, G. S. Wade, and H. M. Woolf, "Combined atmospheric sounding/cloud imagery—a new forecasting tool," *Bull. Amer. Meteor. Soc.*, vol. 66, no. 2, pp. 138–141, Feb. 1985. doi: 10.1175/1520-0477(1985)066<0138:CASINF>2.0.CO;2.

[4] D. Chesters, A. Mostek, and D. A. Keyser, "VAS sounding images of atmospheric stability parameters", *Weather Forecast.*, vol. 1, no. 1, pp. 5–22, Jun. 1986. doi: 10.1175/1520-0434(1986)001<0005:VSIOAS>2.0.CO;2.

[5] A. Mostek, L. W. Uccellini, R. A. Petersen, and D. Chesters, "Assessment of VAS soundings in the analysis of a preconvective environment," *Mon. Weather Rev.*, vol. 114, no. 1, pp. 62–87, Jan. 1986. doi: 10.1175/1520-0493(1986)114<0062:AOVSIT>2.0.CO;2.

[6] W. P. Menzel, F. C. Holt, T. J. Schmit, R. M. Aune, A. J. Schreiner, G. S. Wade, and D. G. Gray, "Application of GOES-8/9 soundings to weather forecasting and nowcasting," *Bull. Amer. Meteor. Soc.*, vol. 79, no. 10, pp. 2059–2077, Oct. 1998. doi: 10.1175/1520-0477(1998)079<2059:AOGSTW>2.0.CO;2.

[7] J. F. Dostalek and T. J. Schmit, "Total precipitable water measurements from GOES sounder derived product imagery," *Weather Forecast.*, vol. 16, no. 5, pp. 573–587, Oct. 2001. doi: 10.1175/1520-0434(2001)016<0573:TPWMFG>2.0.CO;2.

[8] T. J. Schmit, W. F. Feltz, W. P. Menzel, J. Jung, A. P. Noel, J. N. Heil, J. P. Nelson III, and G. S. Wade, "Validation and use of GOES sounder moisture information," *Weather Forecast.*, vol. 17, no. 1, pp. 139–154, Feb. 2002. doi: 10.1175/1520-0434(2002)017<0139:VAUOGS>2.0.CO;2.

[9] Z. Li, J. Li, W. P. Menzel, T. J. Schmit, J. P. Nelson III, J. Daniels, and S. A. Ackerman, "GOES sounding improvement and applications to severe storm nowcasting," *Geophys. Res. Lett.*, vol. 35, no. 3, Feb. 2008, Art. no. L03806. doi: 10.1029/2007GL032797.

[10] T. J. Schmit, J. Li, J. J. Gurka, M. D. Goldberg, K. J. Schrab, J. Li, and W. F. Feltz, "The GOES-R Advanced Baseline Imager and the continuation of current sounder products." *J. Appl. Meteor. Climat.*, vol. 47, no. 10, pp. 2696-2711, Oct. 2008. doi: 10.1175/2008JAMC1858.1.

[11] H. Xie *et al.*, "Integration and ocean-based prelaunch validation of GOES-R Advanced Baseline Imager legacy atmospheric products," *J. Atmos. Ocean. Tech*., vol. 30, no. 8, pp. 1743–1756, Aug. 2013. doi: 10.1175/JTECH-D-12-00120.1.

[12] M. Koenig and E. De Coning, "The MSG global instability indices product and its use as a nowcasting tool," *Weather Forecast.*, vol. 24, no. 1, pp. 272–285, Feb. 2009. doi: 10.1175/2008WAF2222141.1.

[13] Z. Li, J. Li, W. P. Menzel, J. P. Nelson III, T. J. Schmit, E. Weisz, and S. A. Ackerman, "Forecasting and nowcasting improvement in cloudy regions with high temporal GOES sounder infrared radiance measurements," *J. Geophys. Res. Atmos.*, vol. 114, May 2009, Art. no. D09216. doi: 10.1029/2008JD010596.

[14] F. Weng, X. Zou, X. Wang, S. Yang, and M. D. Goldberg, "Introduction to Suomi National Polar-orbiting Partnership Advanced Technology Microwave Sounder for numerical weather prediction and tropical cyclone applications," *J. Geophys. Res. Atmos.*, vol. 117, Oct. 2012, Art. no. D19112. doi: 10.1029/2012JD018144.

[15] F. Weng, X. Zou, N. Sun, H. Yang, M. Tian, W. J. Blackwell, X. Wang, L. Lin, and K. Anderson, "Calibration of Suomi National Polar-orbiting Partnership Advanced Technology Microwave Sounder," *J. Geophys. Res. Atmos.*, vol. 118, pp. 11187–11200, Oct. 2013. doi: 10.1002/jgrd.50840.

[16] A. Gambacorta, "The NOAA unique CrIS/ATMS processing system (NUCAPS): Algorithm theoretical basis documentation," version 1.0, NOAA, College Park, MD, USA, 2013, pp. 3-5; 51-64. [Online]. Available: http://www.ospo.noaa.gov/Products/atmosphere/soundings/nucaps/docs/NUCAPS_ATBD_20130821.pdf

[17] C. Tan *et al.* The Preprocessor of the NOAA Unique CRIS/ATMS Processing System (NUCAPS). Presented at the *STAR JPSS 2015 Annual Science Team Meeting*, College Park, MD, USA, 2015 [Online]. Available: https://www.star.nesdis.noaa.gov/star/documents/meetings/2015JPSSAnnual/Posters/05_PosterI_Tan.pdf.

[18] W. L. Smith *et al.*, "Technical note: Evolution, current capabilities, and future advance in satellite nadir viewing ultraspectral IR sounding of the lower atmosphere," *Atmos. Chem. Phys.*, vol. 9, no. 15, pp. 5563–5574, Aug. 2009. doi: 10.5194/acp-9-5563-2009.

[19] D. Tobin *et al.*, "Suomi-NPP CrIS radiometric calibration uncertainty," *J. Geophys. Res. Atmos.*, vol. 118, no. 18, pp. 10589–10600, Sep. 2013. doi: 10.1002/jgrd.50809.

[20] V. Zavyalov *et al.*, "Noise performance of the CrIS instrument," *J. Geophys. Res. Atmos.*, vol. 118, pp. 13108–13120, Dec. 2013. doi: 10.1002/2013JD020457.

[21] N. Smith, W. L. Smith, E. Weisz, and H. E. Revercomb, "AIRS, IASI, and CrIS Retrieval Records at Climate Scales: An investigation into the propagation of systematic uncertainty," *J. Appl. Meteor. Climatol.*, vol. 54, no. 7, pp. 1465-1481, Jul. 2015. doi: 10.1175/JAMC-D-14-0299.1.

[22] Y. Han *et al.*, "Suomi NPP CrIS measurements, sensor data record algorithm, calibration and validation activities, and record data quality," *J. Geophys. Res. Atmos.*, vol. 118, no. 22, pp. 12734–12748, Nov. 2013. doi: 10.1002/2013JD020344.

[23] J. Susskind, C. D. Barnet, and J. M. Blaisdell, "Retrieval of atmospheric and surface parameters from AIRS/AMSU/HSB data in the presence of clouds," *IEEE Trans. Geosci. Remote Sens.*, vol. 41, no. 2, pp. 390–409, Feb. 2003. doi: 10.1109/TGRS.2002.808236.

[24] J. Susskind, J. Blaisdell, L. Iredell, and F. Keita, "Improved temperature sounding and quality control methodology using AIRS/AMSU data: The AIRS science team version 5 retrieval algorithm," *IEEE Trans. Geosci. Remote Sens.*, vol. 49, no. 3, pp. 883–907, Mar. 2011. doi: 10.1109/TGRS.2010.2070508.

[25] A. Gambacorta *et al.*, "An Experiment Using High Spectral Resolution CrIS Measurements for Atmospheric Trace Gases: Carbon Monoxide Retrieval Impact Study," *IEEE Geosci. Remote Sens. Lett.*, vol. 11, no. 9, pp. 1639-1643, Sep. 2014. doi: 10.1109/LGRS.2014.2303641.

[26] M. D. Goldberg, Y. Qu, L. M. McMillin, W. Wolf, L. Zhou, and M. Divakarla, "AIRS near-real-time products and algorithms in support of operational numerical weather prediction," *IEEE Trans. Geosci. Remote Sens.*, vol. 41, no. 2, pp. 379-389, Feb. 2003. doi: 10.1109/tgrs.2002.808307.

[27] A. Gambacorta and C. D. Barnet, "Methodology and information content of the NOAA NESDIS operational channel selection for the

Cross-Track Infrared Sounder (CrIS)," *IEEE Trans. Geosci. Remote Sens.*, vol. 51, no. 6, pp. 3207-3216, Jun. 2013. doi: 10.1109/TGRS.2012.2220369.

[28] A. Gambacorta, "Status of the NUCAPS Full Spectral Resolution trace gas products," presented at the *STAR JPSS 2017 Annual Science Team Meeting*, College Park, MD, USA, Aug. 14-18, 2017.

[29] A. B. Tanner *et al.*, "Initial Results of the Geostationary Synthetic Thinned Array Radiometer (GeoSTAR) Demonstrator Instrument," *IEEE Trans. Geosci. Remote Sens.*, vol. 47, no. 7, pp. 1947-1957, Jun. 2007. doi: 10.1109/TGRS.2007.894060.

[30] R. A. Peppler, "A review of static stability indices and related thermodynamic parameters," Illinois State Water Survey Division, Climate and Meteorology Section. Champaign, IL, USA. SWS Misc. Publ. 104, Oct. 1988. [Online]. Available: http://www.isws.illinois.edu/pubdoc/mp/iswsmp-104.pdf

[31] R. H. Johns and C. A. Doswell, "Severe Local Storms Forecasting," *Weather Forecast.*, vol. 7, no. 4, pp. 588–612, Dec. 1992. doi: 10.1175/1520-0434(1992)007<0588:SLSF>2.0.CO;2.

[32] A. J. Haklander and A. Van Delden, "Thunderstorm predictors and their forecast skill for the Netherlands," *Atmos. Res.*, vol. 67, pp. 273–299, 2003. doi: 10.1016/S0169-8095(03)00056-5.

[33] A. K. Showalter, "A stability index for thunderstorm forecasting," *Bull. Amer. Meteor. Soc.*, vol. 34, pp. 250-252, 1953.

[34] J. G. Galway, "The lifted index as a predictor of latent instability," *Bull. Amer. Meteor. Soc.*, vol. 37, no. 10, pp. 528–529, Dec. 1956.

[35] J. J. George, *Weather Forecasting for Aeronautics*. New York, NY, USA: Academic, 1960.

[36] R. C. Miller, "Notes on analysis and severe-storm forecasting procedures of the Military Weather Warning Center," AWS, USAF, Scott AFB, IL, USA, Tech. Rep. 200(R), 1967.

[37] [Online]. Available: http://www.wpc.ncep.noaa.gov/international/gdi/GDI_Manuscript_V20161021.pdf

[38] J. P. Craven, R. E. Jewell, and H. E. Brooks, "Comparison between observed convective cloud base heights and lifting condensation level for two different lifted parcels," *Weather Forecast.*, vol. 17, no. 4, pp. 885-890, Aug. 2002. doi: 10.1175/1520-0434(2002)017<0885:CBOCCB>2.0.CO;2.

[39] R. A. Peppler and P. J. Lamb, "Tropospheric static stability and central North American growing season rainfall," *Mon. Wea. Rev.*, vol. 117, no. 6, pp. 1156–1180, Jun. 1989. doi: 10.1175/1520-0493(1989)117<1156:TSSACN>2.0.CO;2.

[40] [Online]. Available: http://www.wpc.ncep.noaa.gov/international/gdi/GDI_Calculation_Algorithm_20140314.pdf

[41] T. Reale, B. Sun, F. H. Tilley, M. Pettey, "The NOAA Products Validation System (NPROVS)," *J. Atmos. Oceanic Technol.*, vol. 29, no. 5, pp. 629 –645, May 2012. doi: 10.1175/JTECH-D-11-00072.1.

[42] N. R. Nalli *et al.*, "Validation of satellite sounder environmental data records: application to the Cross-track Infrared Microwave Sounder Suite," *J. Geophys. Res. Atmos.*, vol. 118, no. 24, pp. 13628–13643, Dec. 2013. doi: 10.1002/2013JD020436.

[43] B. Ingleby, "An assessment of different radiosonde types 2015/2016," ECMWF Technical Memorandum, no. 807, Aug. 2017. [Online]. Available: https://www.ecmwf.int/sites/default/files/elibrary/2017/17551-assessment-different-radiosonde-types-20152016.pdf

[44] D. Bolton, "The Computation of Equivalent Potential Temperature," *Mon. Wea. Rev.*, vol. 108, no. 7, pp. 1046–1053, Jul. 1980. doi: 10.1175/1520-0493(1980)108<1046:TCOEPT>2.0.CO;2.

[45] C. A. Doswell, J. T. Schaefer, D. W. McCann, T. W. Schlatter, and H. B. Wobus, "Thermodynamic analysis procedures at the National Severe Storms Forecast Center," in *Proc. 9th Conf. on Weather Forecasting and Analysis, Amer. Meteor. Soc.*, Seattle, WA, USA, 1982, pp. 304–309.

[46] N. R. Nalli, A. Gambacorta, Q. Liu, C. D. Barnet, C. Tan, F. Iturbide-Sanchez, T. Reale, B. Sun, and V. R. Morris, "Validation of Atmospheric Profile Retrievals from the SNPP NOAA-Unique Combined Atmospheric Processing System 1. Temperature and Moisture," *IEEE Trans. Geosci. Remote Sens.*, to be published. doi: 10.1109/TGRS.2017.2744558.

[47] B. Sun, A. Reale, F. Tilley, M. Pettey, N. R. Nalli, and C. D. Barnet, "Assessment of NUCAPS S-NPP CrIS/ATMS Sounding Products Using Reference and Conventional Radiosonde Observations," *IEEE J. Sel. Topics Appl. Earth Observ.*, vol. 10, no. 6, pp. 2499-2509, Jun. 2017. doi: 10.1109/JSTARS.2017.2670504.

[48] L. M. Candlish, R. L. Raddatz, M. G. Asplin, and D. G. Barber, "Atmospheric Temperature and Absolute Humidity Profiles over the Beaufort Sea and Amundsen Gulf from a Microwave Radiometer," *J. Atmos. Oceanic Technol.*, vol. 29, no. 9, pp. 1182-1201, Sep. 2012. doi: 10.1175/JTECH-D-10-05050.1.

[49] F. Sanders, "Temperatures of Air Parcels Lifted from the Surface: Background, Application and Nomograms," *Weather Forecast.*, vol. 1, no. 3, pp. 190-205, Dec. 1986. doi: 10.1175/1520-0434(1986)001<0190:TOAPLF>2.0.CO;2.

[50] G. H. Bryan, "On the Computation of Pseudoadiabatic Entropy and Equivalent Potential Temperature," *Mon. Wea. Rev.*, vol. 136, no. 12, pp. 5239-5245, Dec. 2008. doi: 10.1175/2008MWR2593.1.

[51] J. M. Wallace and P. V. Hobbs, *Atmospheric Science: An Introductory Survey*, 2nd ed. San Diego, CA, USA: Academic, 2006, pp. 91-93.

[52] [Online]. Available: http://www.wpc.ncep.noaa.gov/archives/web_pages/sfc/sfc_archive_maps.php?arcdate=05/26/2015&selmap=2015052618&maptype=namussfc.

[53] [Online]. Available: http://www.wpc.ncep.noaa.gov/html/fntcodes2.shtml.

[54] [Online]. Available: http://www.wpc.ncep.noaa.gov/html/stationplot.shtml.

[55] J. McCarthy and S. E. Koch, "The evolution of an Oklahoma dryline. Part I: A meso- and subsynoptic-scale analysis," *J. Atmos. Sci.*, vol. 39, no. 2, pp. 225–236, Feb. 1982. doi: 10.1175/1520-0469(1982)039<0225:TEOAOD>2.0.CO;2.

[56] C. L. Ziegler and E. N. Rasmussen, "The initiation of moist convection at the dryline: Forecasting issues from a case study perspective," *Weather Forecast.*, vol. 13, no. 4, pp. 1106–1131, Dec. 1998. doi: 10.1175/1520-0434(1998)013<1106:TIOMCA>2.0.CO;2.

[57] S. E. Peckham and L. J. Wicker, "The influence of topography and lower-tropospheric winds on dryline morphology," *Mon. Wea. Rev.*, vol. 128, no. 7, pp. 2165–2189, Jul. 2000. doi: 10.1175/1520-0493(2000)128<2165:TIOTAL>2.0.CO;2.

[58] L. M. Miloshevich, H. Vömel, D. N. Whiteman, B. M. Lesht, F. J. Schmidlin, and F. Russo, "Absolute accuracy of water vapor measurements from six operational radiosonde types launched during AWEX-G and implications for AIRS validation," *J. Geophys. Res. Atmos.*, vol. 111, May 2006, Art. no. D09S10. doi: 10.1029/2005JD006083.

[59] B. Sun, A. Reale, D. J. Seidel, and D. C. Hunt, "Comparing radiosonde and COSMIC atmospheric profile data to quantify differences among radiosonde types and the effects of imperfect collocation on comparison statistics," *J. Geophys. Res. Atmos.*, vol. 115, Dec. 2010, Art. no. D23104. doi: 10.1029/2010JD014457.

[60] T. N. Carlson, S. G. Benjamin, G. S. Forbes, and Y.-F. Li, "Elevated mixed layers in the regional severe storm environment: Conceptual model and case studies," *Mon. Wea. Rev.*, vol. 111, no. 7, pp. 1453–1474, Jul. 1983. doi: 10.1175/1520-0493(1983)111<1453:EMLITR>2.0.CO;2.

[61] V. E. Kousky, "Diurnal rainfall variation in the Northeast Brazil," *Mon. Wea. Rev.*, vol. 108, no 4, pp. 488-498, Apr. 1980. doi: 10.1175/1520-0493(1980)108<0488:DRVINB>2.0.CO;2.

[62] M. Garstang, H. L. Massie, J. Halverson, S. Greco, and J. Scala, "Amazon coastal squall lines. Part I: Structure and kinematics," *Mon. Wea. Rev.*, vol. 122, no. 4, pp. 608–622, Apr. 1994. doi: 10.1175/1520-0493(1994)122<0608:ACSLPI>2.0.CO;2.

[63] J. C. P. Cohen, M. A. F. Silva Dias, and C. A. Nobre, "Environmental conditions associated with Amazonian squall lines: A case study," *Mon. Wea. Rev.*, vol. 123, no. 11, pp. 3163–3174, Nov. 1995. doi: 10.1175/1520-0493(1995)123<3163:ECAWAS>2.0.CO;2.

[64] [Online]. Available: https://www.wmo.int/pages/prog/www/ois/volume-a/vola-home.htm

[65] T. T. Fujita, *The downburst: microburst and macroburst*, SMRP Research Paper no. 210. Chicago, IL, USA: University of Chicago, 1985.

[66] K. L. Pryor, "Progress and Developments of Downburst Prediction Applications of GOES." *Weather Forecast.*, vol. 30, no. 5, pp. 1182–1200, Oct. 2015. doi: 10.1175/WAF-D-14-00106.1.

Flavio Iturbide-Sanchez (S'03–M'07) received the B.S.E.E degree in electronics engineering from the Autonomous Metropolitan University, Mexico City, Mexico, in 1999, the M.S.E.E. degree in electrical engineering from the Advanced Studies and Research Center of the National Polytechnic Institute, Mexico City, Mexico, in 2001, and the Ph.D. degree from the University of Massachusetts, Amherst, in 2007, where he was advised by Prof. S. C. Reising and supported by the National Science Foundation. His Ph.D. research focused on the miniaturization, development, calibration, and performance assessment of low-cost and power-efficient microwave radiometers for remote sensing applications.

From 2001 to 2005, he was a Research Assistant with the Microwave Remote Sensing Laboratory, University of Massachusetts, where he performed research on the design, development, and characterization of highly integrated multichip modules and microwave circuits for low-noise, low-power consumption, high-gain, and high-stability microwave radiometers. From 2005 to 2007, he was with the Microwave Systems Laboratory, Colorado State University, Fort Collins, focusing on development, characterization, calibration, and deployment of the low-cost and power-efficient Compact Microwave Radiometer for Humidity profiling (CMR-H). Since 2008, he has been with the I. M. Systems Group, Inc., at the NOAA/NESDIS/Center for Satellite Applications and Research, College Park, MD supporting the development of operational physical retrieval systems that employ hyperspectral-infrared and microwave observations implemented for the NOAA Polar Operational Environmental Satellites project, the National Polar-orbiting Operational Environmental Satellite System, and the Joint Polar Satellite System. His research interests include satellite remote sensing, satellite data assimilation, inverse theory applied to geoscience fields, weather forecasting, Earth system science, small satellites and emerging technologies for Earth observations.

Dr. Iturbide-Sanchez won a First-Place Poster Award at the 11th Specialist Meeting on Microwave Radiometry and Remote Sensing Applications (MicroRad 2010) in Washington, DC. While a Ph.D. student, he was a finalist in two IEEE Student Paper Competitions, one at the International Geoscience and Remote Sensing Symposium in Anchorage, AK, September 2004 and one at the International Microwave Symposium in San Francisco, CA, June 2006. He was also awarded the Mexican National Council for Science and Technology (CONACYT) Graduate Fellowship from 1999 to 2004.

Silvia R. Santos da Silva received the B.S. degree in meteorology from the Federal University of Rio de Janeiro, Rio de Janeiro, Brazil, in 2002, and the M.S. degree in atmospheric and oceanic science from the University of Maryland, College Park, MD, USA, in 2016.

From 2014 to 2016, she was awarded a Graduate Scholarship from the CAPES Foundation/Ministry of Education of Brazil through the Brazil Scientific Mobility Program. She is currently pursuing the Doctor of Philosophy degree in atmospheric and oceanic science at the University of Maryland, College Park, where she is involved in multidisciplinary integrated assessments of the interaction between water, climate, land and energy processes with a special focus in Latin America.

With years of work experience in the operational weather forecasting at the Brazilian Navy Marine Meteorological Service, her additional research interests include applying and developing satellite-derived products to improve the operational weather forecasting, and for climate applications.

Quanhua Liu received the B.S. degree from the Nanjing University of Information Science and Technology, Nanjing, China, in 1982, the master's degree in physics from the Chinese Academy of Science, Beijing, China, in 1984, and the Ph.D. degree in meteorology and remote sensing from the University of Kiel, Kiel, Germany, in 1991. He is currently a Physical Scientist with the National Oceanic and Atmospheric Administration Center for Satellite Application and Research, National Environmental Satellite, Data, and Information Service, College Park, MD, USA, where he is involved in advanced technology microwave sounder sensor data calibration and microwave integrated retrieval system. He has contributed to the development of the community radiative transfer model that operationally supports satellite radiance assimilation for weather forecasting and the Joint Polar Satellite System/SuomiNational Polar-orbiting Partnership and GOES-R missions for instrument calibration, validation, long-term trend monitoring, and satellite retrieved products.

Kenneth L. Pryor received a B.A. degree in Interdisciplinary Studies from Virginia Tech in 1989, a Certificate in Broadcast Meteorology from Mississippi State University in 1995, and an M.S. degree in Meteorology from University of Maryland, College Park, in 2004.

He served four years in the U.S. Navy from 1989 to 1993, including duty as Weather Officer on the USS San Diego (AFS-6). After his naval service, Ken was employed as a weather observer and forecaster for the National Weather Service and U.S. Air Force. In NESDIS Center for Satellite Applications and Research since 2000, Ken has pursued research in severe convective storms and downbursts and has developed Geostationary Operational Environmental Satellite (GOES) derived index products to assess the potential severity of convective downbursts. In addition, Ken is a Virtual Institute for Satellite Integration Training (VISIT) instructor where he presents the web-based teletraining module "Forecasting Convective Downburst Potential Using GOES Sounder Derived Products" and has trained over 800 forecasters in techniques for predicting downburst risk using GOES sounder derived product data.

Michael E. Pettey received the B.S degree in computer science from the University of Maryland, College Park, Maryland, USA in 1989. He received the M.S. degree in computer science from Johns Hopkins University, Baltimore, Maryland, USA in 1999.

He currently serves as a Senior Graphics Systems Analyst with I.M. Systems Group, College Park, Maryland, USA under contract with the NOAA/NESDIS Center for Satellite Applications and Research (formerly the Office of Research and Applications). He is the lead designer and developer of a suite of graphical programs that provide researchers and

scientists with the ability to view and analyze data produced by the NOAA Products Validation System (NPROVS). His other responsibilities include capturing satellite data from many disparate sources and preparing the data for inclusion within NPROVS.

Nicholas R. Nalli received the B.S. and M.S. degrees in science education from the State University of New York (SUNY), College at Oneonta, Oneonta, NY, USA, in 1988 and 1989, respectively, and the M.S. and Ph.D. degrees in atmospheric and oceanic sciences from the University of Wisconsin (UW)-Madison, Madison, WI, USA, in 1995 and 2000, respectively. He studied earth sciences at SUNY-Oneonta with a focus on meteorology and minor in mathematics, and minored in physics at UW-Madison.

He was awarded a four-year Postdoctoral Fellowship with the Cooperative Institute for Research in the Atmosphere, Colorado State University, which he completed onsite at the NOAA/NESDIS Center for Satellite Applications and Research (STAR), Silver Spring, MD, USA (formerly the Office of Research and Applications), as a Visiting Scientist. He is currently a Senior Research Scientist (onsite contractor) at STAR, where he performs applied and basic research. His primary research specialties include environmental satellite remote sensing, infrared radiative transfer, and validation, with focus on oceanic and atmospheric applications. Other research interests include atmospheric aerosols, cloud morphology, air–sea interactions, boundary layer and marine meteorology, oceanographic intensive field campaigns, forensic science, and global climate change applications.

Dr. Nalli has participated in 14 oceanographic research expeditions onboard research vessels that have acquired data in support of diverse research applications, including instrument proofs-of-concept (e.g., the marine atmospheric emitted radiance interferometer), sea surface emissivity model development, observation of marine meteorological phenomena (e.g., Saharan air layers, dust and smoke outflows, and atmospheric rivers), and validation of satellite retrieved environmental data records, including sea surface temperature, temperature/moisture/ozone profiles, and hyperspectral infrared cloud-cleared radiances, since 1995. He is a member of both the American Meteorological Society and American Geophysical Union. He also remains interested and active in science education and public outreach.